Radical chemistry at a UK coastal receptor site – Part 1: observations of OH, HO₂, RO₂, and OH reactivity and comparison to MCM model predictions

Robert Woodward-Massey[1], Roberto Sommariva[2,4], Lisa K. Whalley[1,3], Danny R. Cryer[1], Trevor
5 Ingham[1], William J. Bloss[4], Sam Cox[5,a], James D. Lee[6,7], Chris P. Reed[6,b], Leigh R. Crilley[4,c], Louisa J.
Kramer[4,d], Brian J. Bandy[8], Grant L. Forster[9], Claire E. Reeves[8], Paul S. Monks[2], and Dwayne E. Heard[1]

[1]School of Chemistry, University of Leeds, Leeds, LS2 9JT, UK
[2]School of Chemistry, University of Leicester, University Road, Leicester, LE1 7RH, UK
[3]National Centre for Atmospheric Science, University of Leeds, Leeds, LS2 9JT, UK
10 [4]School of Geography, Earth and Environmental Sciences, University of Birmingham, Birmingham, B15 2TT, UK
[5]Research Software Engineering Team, University of Leicester, Leicester, LE1 7RH, UK
[6]Wolfson Atmospheric Chemistry Laboratories, Department of Chemistry, University of York, York, YO10 5DD, UK
[7]National Centre for Atmospheric Science, University of York, York, YO10 5DD, UK
[8]Centre for Ocean and Atmospheric Sciences, School of Environmental Sciences, University of East Anglia, Norwich, UK
15 [9]National Centre for Atmospheric Science, University of East Anglia, Norwich, NR4 7TJ, UK
[a]now at: Digital Research Service, University of Nottingham, Nottingham, NG7 2RD, UK
[b]now at: Faculty for Airborne Atmospheric Measurements, Cranfield University, Cranfield, MK43 0AL, UK
[c]now at: Department of Chemistry, York University, Toronto, M3J 1P3, Canada
[d]now at: Ricardo Energy & Environment, Harwell, Oxfordshire, OX11 0QR, UK

20

Correspondence to: Lisa K. Whalley (l.k.whalley@leeds.ac.uk) and Dwayne E. Heard (d.e.heard@leeds.ac.uk)

Abstract. OH, HO₂, total and partially-speciated RO₂, and OH reactivity (k'_{OH}) were measured during the July 2015 ICOZA
(Integrated Chemistry of OZone in the Atmosphere) project that took place at a coastal site in North Norfolk, UK. Maximum
measured daily OH, HO₂, and total RO₂ radical concentrations were in the range 2.6–17 × 10⁶, 0.75–4.2 × 10⁸, and 2.3–8.0 ×
25 10⁸ molecule cm⁻³, respectively. k'_{OH} ranged from 1.7 to 17.6 s⁻¹ with a median value of 4.7 s⁻¹. ICOZA data were split by
wind direction to assess differences in the radical chemistry between air that had passed over the North Sea (NW–SE sectors)
or major urban conurbations such as London (SW sector). A photostationary steady-state (PSS) calculation underpredicted
daytime OH in NW–SE air by ~35%, whereas agreement (~15%) was found within instrumental uncertainty (~26% at 2σ) in
SW air. A box model using MCMv3.3.1 chemistry was in better agreement with the OH measurements, but it overpredicted
30 HO₂ observations in NW–SE air in the afternoon by a factor of ~2–3, although slightly better agreement was found for HO₂ in
SW air (factor of ~1.4–2.0 underprediction). The box model severely underpredicted total RO₂ observations in both NW–SE
and SW air by factors of ~8–9 on average. Measured radical and k'_{OH} levels and measurement-to-model ratios displayed strong
dependences on NO mixing ratios. The PSS calculation could capture OH observations at high NO but underpredicted the
observations at low NO. The box model overpredicted HO₂ concentrations at low NO in NW–SE air, whereas in SW air, the
35 measurements and model results were in agreement across the full NO range. The box model underpredicted total RO₂ at all

NO levels, where the measurement-to-model ratio scaled with NO. This trend has been found in all previous field campaigns in which total RO_2 was measured using the RO_xLIF technique and suggests that peroxy radical chemistry is not well understood under high NO_x conditions.

1 Introduction

40 The removal of trace gases in the troposphere is dominated by reactions with the hydroxyl radical (OH) during the daytime. At semi-polluted locations, OH formation is mainly initiated by the photolysis of ozone (O_3) and nitrous acid (HONO):

$$O_3 + hv \ (\lambda < 340 \text{ nm}) \rightarrow O(^1D) + O_2 \tag{R1a}$$

$$O(^1D) + H_2O \rightarrow OH + OH \tag{R1b}$$

45 $$O(^1D) + M \rightarrow O(^3P) + M \tag{R1c}$$

$$HONO + hv \ (\lambda < 400 \text{ nm}) \rightarrow OH + NO \tag{R2}$$

The OH oxidation of volatile organic compounds (VOCs) in the presence of oxygen results in the formation of organic peroxy radicals (RO_2):

50

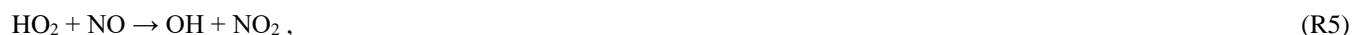$$OH + RH + O_2 \rightarrow RO_2 + H_2O \tag{R3}$$

RO_2 radicals may also be formed from the photolysis of oxygenated VOCs (OVOCs). In the presence of NO, RO_2 radicals produce hydroperoxyl radicals (HO_2) and carbonyl species:
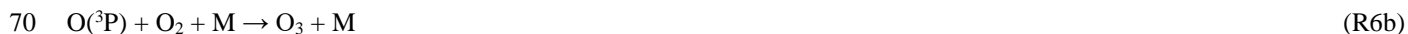
55

$$RO_2 + NO \rightarrow RO + NO_2 \tag{R4a}$$

$$RO + O_2 \rightarrow R'CHO + HO_2 \tag{R4b}$$

HO_2 also reacts with NO to reform OH:

60

$$HO_2 + NO \rightarrow OH + NO_2 \ , \tag{R5}$$

thus completing the atmospheric reaction cycle known as the hydrogen oxide ($HO_x = OH + HO_2$) cycle. HO_2 is also formed by formaldehyde (HCHO) photolysis and by reaction of OH with CO and HCHO. Non-photolytic sources of radicals include

65 nitrate radical (NO_3) chemistry and the ozonolysis of alkenes. Chlorine atoms may also react with VOCs to generate RO_2 radicals. The subsequent photolysis of NO_2 formed in reactions (R4a) and (R5) results in the production of ozone in the troposphere:

$$NO_2 + h\nu \ (\lambda < 400 \text{ nm}) \rightarrow O(^3P) + NO \qquad\qquad\qquad\qquad (R6a)$$

70 $$O(^3P) + O_2 + M \rightarrow O_3 + M \qquad\qquad\qquad\qquad\qquad\qquad (R6b)$$

The short lifetimes of OH, HO$_2$, and RO$_2$, collectively known as RO$_x$, make them ideal species to test our understanding of tropospheric oxidation chemistry, particularly when measurements of OH reactivity (the inverse of the OH lifetime, k'_{OH}) are also available.

75   The marine boundary layer (MBL) accounts for a substantial fraction (71%) of the planetary boundary layer. Field measurements of OH and HO$_2$ radicals in the MBL have shown that in general, models are capable of simulating the observed concentrations to within ~30% or better. The majority of these studies were characterised by clean air masses with very low to relatively low NO mixing ratios (Sommariva et al., 2004; Heard et al., 2006; Mao et al., 2009; Whalley et al., 2010; Beygi et al., 2011; Vaughan et al., 2012; Mallik et al., 2018), where observed OH and HO$_2$ concentrations were generally in the range

80   ~3–8 × 10^6 molecule cm^{-3} and ~1–4 × 10^8 molecule cm^{-3}, respectively. In the MBL, HO$_x$ radical production is normally dominated by the reaction of O(^{1}D) with water vapour (reaction (R1)), but HCHO photolysis to HO$_2$ is often an important primary radical source (Ren et al., 2008; Stone et al., 2018). Similarly, owing to low primary VOC levels, OVOCs other than HCHO can account for a significant proportion of OH reactivity (Sommariva et al., 2006; Mao et al., 2009; Whalley et al., 2010; Stone et al., 2018) , and can also be important radical sources. HO$_x$ chemistry was shown to be sensitive to halogen

85   chemistry in some studies (Bloss et al., 2005b; Whalley et al., 2010; Stone et al., 2018), particularly with regard to the partitioning between OH and HO$_2$ since BrO and IO radicals act to convert HO$_2$ to OH (Sommariva et al., 2006). Heterogeneous uptake of HO$_2$ on aerosols can be a significant HO$_x$ loss route under low NO conditions (Sommariva et al., 2004; Sommariva et al., 2006; Whalley et al., 2010; Stone et al., 2018), but considerable uncertainty surrounds the treatment of heterogeneous processes such as the parameterisation of uptake coefficients (γ_{HO2}) (Song et al., 2020), which historically

90   have sometimes been set to unrealistically high values to achieve measurement-model agreement.

  To the authors' knowledge, there are no reported field campaigns in the MBL in which OH, HO$_2$, RO$_2$, and k'_{OH} were all measured simultaneously. Similarly, there are only two studies (Novelli et al., 2014a; Mallik et al., 2018) in the MBL in which OH measurements made by laser-induced fluorescence (LIF) used a technique that allows for the discrimination of OH measurement interferences (Mao et al., 2012). The interferences may arise from both known (e.g., stabilised Criegee

95   intermediates (Novelli et al., 2014b), NO$_3$ radicals (Fuchs et al., 2016)) and unknown species. In this work, we present interference-free measurements of OH (Woodward-Massey et al., 2020) alongside HO$_2$, total and partially-speciated RO$_2$, and k'_{OH} from a field campaign at a UK coastal receptor site. This complete suite of RO$_x$ measurements allowed for more comprehensive testing of our understanding of MBL chemistry through comparisons to the predictions of a box model. The field campaign took place at a site subject to a variety of air mass types, at which previous field campaigns with (incomplete)

100 RO$_x$ and/or k'_{OH} measurements were conducted in 1994–1995 (Forberich et al., 1999; Grenfell et al., 1999; Penkett et al., 1999), 2002 (Fleming et al., 2006; Green et al., 2006), and 2004 (Smith, 2007; Lee et al., 2009b).

2 The Integrated Chemistry of OZone in the Atmosphere (ICOZA) project

The ICOZA field campaign focussed on the chemistry surrounding the production of ozone, which is harmful to human health (Jerrett et al., 2009), damages vegetation (Krupa et al., 1998), and is a potent greenhouse gas (Ipcc, 2014). The ICOZA

105   campaign took place in June–July 2015 at the Weybourne Atmospheric Observatory (WAO), which is a Global Atmospheric Watch (GAW) regional station run by the University of East Anglia (UEA) on behalf of the National Centre for Atmospheric Science (https://weybourne.uea.ac.uk/). As shown in Figure 1, the site is located on the North Norfolk Coast, UK (52°57'02" N, 1°07'19"E), ~50 km NNW of Norwich and ~190 km NE of London. The site is situated 16 m above sea level and is surrounded by grass fields on three sides, with the fourth facing due north towards a gently-sloped pebble beach. The nearest

110   major road is a rural road (A147) located ~800 m to the south.

As the site is situated on the North Sea coast, it is subject to clean air masses that have travelled over the North Sea and originating from polar regions, as well as more polluted air that has been influenced by emissions from major UK cities (e.g., London, Birmingham) ~12–24 h before arriving at the site (Lee et al., 2009b). Polluted continental air, containing aged (by up to 36 hours) anthropogenic emissions from continental Europe, may also be sampled (Lee et al., 2009b). In addition, the site

115   is subject to emissions from local roads, as well as shipping influences (Cárdenas et al., 1998).

The campaign began on 1st July 2015, but radical measurements commenced on the afternoon of 29th June. The last radical observations were made during the early morning of 22nd July, before the campaign end date of 31st July.

2.1 Instrumentation

A list of the instrumentation involved in measurements of trace gases, aerosols, and photolysis frequencies during the ICOZA

120   campaign is given in Table 1. Instruments sampled ambient air from a height of ~4 m from the roofs of individual shipping containers (Universities of Leeds and Leicester), a van (Birmingham), and from either the roof (~5 m) of the main WAO building directly, or via a common glass manifold (glass, ~15 cm ID) located on a tower that reached ~10 m above the roof. Comparisons of NO_x observations, measured using multiple instruments, indicated no significant heterogeneity in the air sampled from different positions of the site.

2.1.1 The Leeds ground-based FAGE instrument

125

OH, HO_2, and RO_2 radicals were measured using the fluorescence assay by gas expansion (FAGE) technique (Hard et al., 1984; Heard and Pilling, 2003). The University of Leeds ground-based FAGE instrument, which has been described in detail elsewhere (Creasey et al., 1997; Whalley et al., 2010; Whalley et al., 2013; Whalley et al., 2018; Woodward-Massey, 2018; Woodward-Massey et al., 2020), has been deployed in ~25 intensive field campaigns since 1996 in a variety of chemical

130   environments. The instrument was used to measure OH and HO_2 during a previous campaign at the WAO, namely the Tropospheric ORganic photoCHemistry experiment (TORCH) 2 campaign (Smith, 2007).

Atmospheric
Chemistry
and Physics
Discussions

Only a brief description of the instrument is given here. Ambient OH concentrations are measured using laser-induced fluorescence (LIF) spectroscopy. The inlet consists of a conical turret (4 cm length, 3.4 cm ID) with a 1.0 mm diameter pinhole through which ambient air is sampled at ~7 slm. The turret is mounted on top of a stainless steel fluorescence cell (HO_x cell),

135 which is held at ~1.5 Torr (~2 hPa) using a combination of a Roots blower (Leybold RUVAC WAU 10001) and a rotary pump (Leybold SOGEVAC SV2000). A wavelength tuneable solid-state laser (YAG pumped Ti Sapphire laser) with a pulse repetition frequency of 5 kHz is tuned to the OH $A^2\Sigma^+$ (v′ = 0) ← $X^2\Pi_{3/2}$(v″ = 0) electronic transition at λ = 308 nm. Approximately 10–20 mW of laser light is supplied to the fluorescence cell using an optical fibre. OH fluorescence near 308 nm is detected with a micro-channel plate photomultiplier (MCP, Photek PMT325/Q/BI/G with 10 mm diameter photocathode),

140 which is used together with a 50 ns gating unit (Photek GM10-50) and a 2 GHz 20 dB gain amplifier (Photek PA200-10). Due to failures of the MCP detectors used during ICOZA, channel photomultiplier (CPM, Perkin Elmer 993P) detectors were sometimes used for the RO_x fluorescence cell (see below). Fluorescence signals from the MCP/CPM detectors are analysed using gated photon counting.

HO$_2$ is detected after conversion to OH by the addition of NO (BOC, 99.95%) delivered using a mass flow controller

145 (MFC, MKS Instruments 1179A series). An advantage for ICOZA relative to TORCH 2 and other previous field campaigns is the addition of instrumental capability for observations of RO_2 radicals, using the RO_xLIF technique (Fuchs et al., 2008), as well as interference-free measurements of HO_2 (Fuchs et al., 2011; Whalley et al., 2013). The Leeds group first applied the RO_xLIF method to ambient RO_2 observations in London (Whalley et al., 2018) and has since deployed this approach in Beijing (Slater et al., 2020; Whalley et al., 2020). The RO_xLIF method relies on the reactions of RO_2 radicals with NO (BOC, 500

150 ppmv in N_2) and CO (BOC, 5% in N_2) in a flow tube held at ~30 Torr, which result in initial conversion of RO_2 to OH (RO_2 + NO → HO_2, HO_2 + NO → OH) and then to HO_2 (OH + CO → HO_2; very rapid conversion back to HO_2 results in minimal radical wall losses) that is finally detected as OH via addition of NO inside a second FAGE cell (RO_x cell) that the RO_2 flow tube is coupled to. During fieldwork, the two FAGE cells are used to make sequential measurements of OH, HO_2, HO_2^* (HO_2 plus an interference from RO_2 radicals derived from long-chain alkanes and alkene and aromatic species; see Whalley et al.

155 (2013) for full details), and total RO_2 in the following data acquisition cycle: (1) the first cell (HO_x) measures OH while simultaneously the second cell (RO_x) measures HO_2^* (high NO flow, 50 sccm; RO_2 interference maximised), (2) the HO_x cell measures HO_2 (low NO flow, 5 sccm; RO_2 interference minimised) while the RO_x cell measures total RO_2. The RO_xLIF method allows for the speciation of total RO_2 into "complex" (cRO_2) and "simple" (sRO_2) RO_2 types (Whalley et al., 2013; Tan et al., 2017; Whalley et al., 2018). cRO_2 are those that readily convert to OH in HO_2^* mode (cRO_2 = HO_2^* − HO_2; note

160 that in other previous studies, cRO_2 have also been labelled as $RO_2^\#$ or RO$_2$i), and correspond to RO_2 radicals derived from alkenes, aromatics, and long-chain (> C_3) alkanes. sRO_2 concentrations are derived from the difference between total RO_2 and cRO_2 and correspond to RO_2 radicals derived from small-chain (< C_4) alkanes. For more details of the speciation of sRO_2 and cRO_2, the reader is referred to Whalley et al. (2013) and Whalley et al. (2018).

Background signals are normally obtained by scanning the laser wavelength to a position that is off-resonance from the

165 OH transition line. In the case of OH, this yields the measurement referred to as OHwave (Mao et al., 2012). Alternatively, the

Atmospheric
Chemistry
and Physics
Discussions

OH background may be determined chemically, via addition of an OH scavenger (e.g., propane) prior to FAGE sampling, which results in an OH measurement known as OHchem (Mao et al., 2012). The recording of OHchem can be used to test for the presence of interferences in conventional OHwave detection. Prior to the ICOZA campaign, an inlet pre-injector (IPI) module (Novelli et al., 2014a) was constructed to facilitate OHchem measurements in the Leeds FAGE system (Woodward-

170 Massey et al., 2020). The IPI module was first deployed for ambient measurements of OHchem during ICOZA. To test for interferences, two IPI sampling periods were conducted in the middle of the campaign, separated by a few days (3rd–8th July and 12th–16th July). A comparison of OHwave (corrected for the small and well-characterised interference from $O(^1D) + H_2O$, with $O(^1D)$ deriving from laser photolysis of O_3 (Woodward-Massey et al., 2020)) and OHchem measurements yielded a slope (OHwave vs OHchem) of 1.16 ± 0.06, with the non-unity value suggesting the presence of a small unknown OHwave

175 interference during ICOZA on the order of 10–20%, which is smaller than the overall measurement accuracy of 26% at 2σ. The OH data presented in this work correspond to OHchem when such data were available, but OHwave otherwise, where all OHwave data have been corrected for the known interference from O_3/H_2O. No attempt has been made to correct the OHwave data for the presence of other unknown interferences, which must be considered as an additional uncertainty in our analyses.

The Leeds FAGE instrument was calibrated by supplying known radical concentrations to the instrument inlets. Radicals

180 were delivered in an excess flow (~40 slm) of humidified synthetic air (BOC, BTCA 178) using a turbulent flow tube. OH and HO_2 were generated in a 1:1 ratio (Fuchs et al., 2011) by the photolysis of water vapour at 184.9 nm using a Hg(Ar) pen-ray lamp (LOT LSP035). For RO_2 calibrations, CH_4 (BOC, CP grade 99.5%) was added to form HO_2 and CH_3O_2 in a 1:1 ratio. To enable the calculation of radical concentrations, N_2O (BOC, medical grade 98%) chemical actinometry (Edwards et al., 2003; Faloona et al., 2004) was performed before and after the campaign in order to determine the product of the lamp flux at

185 184.9 nm and the photolysis time in the flow tube. Multipoint calibrations were performed for all radical species at regular intervals during the campaign, approximately once per week. The calibration factors (i.e., sensitivities) obtained did vary somewhat due to instrumental issues, namely the need to switch between MCP/CPM detectors. One calibration factor was applied to periods in which an MCP was used, and one for periods in which a CPM was used, where both calibration factors were derived from the average sensitivities of multiple MCP or CPM calibrations. As a consequence of the detector changes,

190 limits of detection (LODs) also varied over the course of ICOZA, with campaign-median 5 min LODs ($\pm 1\sigma$) of $(6.1 \pm 4.1) \times 10^5$, $(4.0 \pm 2.7) \times 10^6$, and $(5.0 \pm 1.2) \times 10^7$ molecule cm^{-3} for OH, HO_2, and total RO_2, respectively, for a signal-to-noise ratio (SNR) of 2.

2.1.2 The Leeds OH reactivity instrument

The Leeds shipping container also housed an instrument used for the measurement of total OH reactivity, k'_{OH}. Full details

195 may be found in Cryer (2016) and Stone et al. (2016) but the key features are described here. The instrument consists of an atmospheric pressure flow tube (85 cm length, 5 cm ID) coupled to an OH fluorescence cell, which was located on the roof of the Leeds container during the ICOZA field campaign. The low pressure in the fluorescence cell (~2 Torr) is provided by the same pumping system as the FAGE cells. The flow tube samples air (via ½" PFA tubing) from close to the FAGE inlets at ~16

slm using a vacuum pump (Agilent Technologies IDP-3 Dry Scroll Pump). The laser flash photolysis pump and probe

200 technique is used here (Jeanneret et al., 2001; Sadanaga et al., 2004), which involves the 266 nm laser (Quantel USA CFR 200) photolysis (pump) of ambient O_3 to generate OH via the reaction of $O(^1D)$ with H_2O. The OH signal decay is then observed in real time by LIF (the probe). Fitting of the first-order exponential obtained yields k'_{OH}, after subtraction of the physical decay rate controlled by non-chemical losses of OH (e.g., diffusion). 308 nm probe light is generated using the laser system described above. Previously, OH reactivity was measured at the WAO during TORCH 2 using a different method, the

205 sliding injector technique with FAGE detection of OH (Ingham et al., 2009; Lee et al., 2009b).

2.1.3 Supporting measurements

Formaldehyde (HCHO) was measured using an LIF instrument developed in Leeds, full details of which may be found in Cryer (2016). The instrument is based on the design of Hottle et al. (2009) and uses a pulsed (300 kHz) tuneable fibre laser (TFL3000, Novawave) to generate UV radiation at 353.370 nm, which excites the HCHO $5_{0,5} \leftarrow 5_{1,4}$ rotational transition of

210 the 4 $A^1A_2 \leftarrow X^1A_1$ vibronic band. As with FAGE, gas is sampled into a low-pressure detection cell (110–120 Torr), but broadband fluorescence is collected at red-shifted wavelengths ($\lambda \sim 390$–550 nm). The fluorescence detected using a PMT (Sens-Tech P25PC photodetector module) and the signal recorded by gated photon counting (PMS400A, Becker and Hickl). The background is determined by moving the laser wavelength to an offline position ($\lambda = 353.360$ nm). The compact HCHO instrument is housed in a shock-insulated 19" rack inside a plastic case, which was situated in the main WAO building during

215 ICOZA and sampled air through the common glass manifold at a height of ~15 m. HCHO was also measured using Hantzsch colourimetry (Nash, 1953), with reasonably good agreement between the two techniques as demonstrated by the fit $[HCHO]_{LIF}$ $= 1.2 \times [HCHO]_{Hantzch} + 0.3$ ppbv ($R^2 = 0.77$; data not shown).

Photolysis frequencies (J) for a variety of species, including $O_3 \rightarrow O(^1D)$, NO_2, H_2O_2, HONO, HNO_3, and HCHO, were calculated using the actinic flux measured using a 2π spectral radiometer and published absorption cross-sections and

220 photodissociation quantum yields; $J(O^1D)$ was also measured using a 2π filter radiometer (Meteorologie Consult GmbH) (Bohn et al., 2008). A variety of other supporting instruments (Table 1) were brought to the WAO site. Observational data were also provided by instruments permanently located at WAO (e.g., CO, NO_x, O_3, SO_2, VOCs, meteorological data; see Table 1).

2.2 Model description

225 In this work, radical concentrations were compared to the predictions of a zero-dimensional box model incorporating a kinetic and photochemical mechanism, the Master Chemical Mechanism (MCM, http://mcm.leeds.ac.uk/MCM)(Saunders et al., 1997; Jenkin et al., 2003; Saunders et al., 2003). The current version of the MCM was used, v3.3.1 (Jenkin et al., 2015). The MCM is a near-explicit chemical mechanism, which represents the oxidative degradation of methane and 142 primary emitted VOCs and incorporates ~17 000 reactions of ~6700 closed shell and free radical species. A subset of the MCM with 4258 species

230 and 12 851 reactions was used instead of the full MCM, reflecting the suite of VOC measurements during ICOZA (Table 1), e.g., no measurements of $> C_6$ alkanes, and limited BVOC observations (discussed below).

The MCM model simulations were conducted using AtChem2 (https://github.com/AtChem/AtChem2; (Sommariva et al., 2020)). Three model scenarios were used for the interpretation of radical observations: MCM-base, MCM-carb, and MCM-hox. The base model, MCM-base, was constrained to all measured trace gases listed in Table 1, with the exception of radical

235 species (including NO_3 radicals, due to limited measurement data for NO_3), and OH reactivity, Cl_2, HCHO, the sum of methyl vinyl ketone and methacrolein (MVK+MACR), xylenes, monoterpenes, and dimethyl sulphide (DMS). MCM-carb was additionally constrained to measured carbonyl species (HCHO, MVK+MACR), but was otherwise identical to the base model; MVK and MACR (both C_4H_6O, measured as a sum using proton transfer reaction–mass spectrometry (PTR–MS)) were assumed to be present in a 1:1 ratio. Similarly, MCM-hox was the same as the base model but was additionally constrained to

240 FAGE-measured HO_2. In all simulations, the ratio of trimethylbenzene (TMB) isomers (i.e., C_9 aromatics, also indistinguishable by PTR–MS) was assumed to be 1:1:1. In all simulations, NO and NO_2 were constrained as separate species rather than as total NO_x.

Temperature, pressure, and RH were also constrained in the MCM models, along with spectral radiometer measurements of photolysis frequencies: $O_3 \rightarrow O(^1D)$, NO_2, HONO, HNO_3, NO_3, HCHO, CHOCHO, CH_3CHO, CH_3COCH_3, CH_3NO_3,

245 $C_2H_5NO_3$, $1-C_3H_7NO_3$, $2-C_3H_7NO_3$, and $ClNO_2$. For species with more than one photolytic decomposition channel, branching ratios were taken from the MCM, with the exception of CHOCHO (glyoxal, three channels) for which values were corrected with those used in the Tropospheric Ultraviolet and Visible (TUV) radiation model (Madronich, 1992). Photolysis frequencies that were not measured were calculated using the MCM parameterisation, scaled by a factor derived from measured and calculated $J(NO_2)$ to account for cloud cover.

250 All measurement constraints were used at their original time resolution, as described in Sommariva et al. (2020). First-order physical losses of unmeasured, model-generated intermediates (e.g., unmeasured OVOCs, organic nitrates, peroxides, acids, and alcohols) through dry deposition were taken from Zhang et al. (2003), where an environment of deciduous trees and long grass/crops was assumed, representative of the immediate area around the WAO. The boundary layer height was estimated at 800 m and kept constant for the duration of the simulations. As examples, these constraints lead to deposition velocities of

255 ~6.4, ~2.8, and ~2.3 cm s^{-1}, corresponding to first-order deposition lifetimes of ~4, ~10, and ~12 h, for HNO_3, H_2O_2, and HCHO, respectively. The lifetime of these model-generated secondary products was determined by their first-order loss rates of dry deposition, heterogeneous uptake (see below), and photolysis, and bimolecular reactions (e.g., with OH and Cl atoms).

In addition to dry deposition, physical losses to aerosols (i.e., heterogeneous uptake) were considered in all model scenarios, represented by the following first-order loss rate (Ravishankara, 1997):

260

$$k'_{loss} = \omega A \gamma / 4 ,$$ (E1)

where ω is the mean molecular speed of the species being taken up, A is the aerosol surface area measured using an aerodynamic particle sizer (APS, range: <0.5–20 μm), and γ is the aerosol uptake coefficient. Heterogeneous uptake was
265   considered for the following species: O_3, OH, HO_2, H_2O_2, HO_2NO_2, NO, NO_2, HONO, HNO_3, NO_3, N_2O_5, SO_2, SO_3, HCl, Cl, and $ClNO_2$. γ_{HO2} was set to a constant value of 0.1 in all model scenarios, the same value used in analyses of the Clean air for London (ClearfLo) campaign (Whalley et al., 2018).

The model was run for 48 hours (spin-up time) then reinitialised with the values of all species at the end of this period and rerun for the whole campaign. This allowed radical species and other reactive intermediates to reach steady-state levels but
270   prevented the build-up of secondary products. The model output data were averaged to 15 min for the comparisons featured in this work.

OH concentrations can also be calculated using a photostationary steady-state (PSS) approach, which uses field measured quantities only, providing a check on (1) the internal consistency of OH, HO_2, and k'_{OH} observations and (2) whether the OH budget can be balanced using measured quantities. PSS OH was calculated using the following equation:
275

$$[OH]_{PSS} = P_{OH} / k'_{OH} ,\qquad\qquad\qquad (E2)$$

where k'_{OH} is obtained directly from measured OH reactivity; P_{OH} terms accounted for the photolysis of O_3 to $O(^1D)$ (R1a) and reaction with water vapour (R1b), photolysis of HONO (R2), reactions of HO_2 (R5) with NO and O_3, and alkene ozonolysis
280   reactions:

$$P_{OH} = 2J(O^1D)[O_3]\,f + J(HONO)[HONO] + k_{HO2+NO}[HO_2][NO] + k_{HO2+O3}[HO_2][O_3] + \Sigma^i\,k_{O3+ALKi}[O_3][ALK_i]Y^{OH}_{ALKi} ,\quad (E3)$$

where f is the fraction of $O(^1D)$ atoms that react with H_2O to form OH (~10%), $J(HONO)$ is the spectral radiometer-determined
285   HONO photolysis rate, and the final term on the right-hand side accounts for the total OH formation from the ozonolysis of each measured alkene (ALK) i with yield Y^{OH}_{ALKi}. Rate constants and yields were taken from MCMv3.3.1 (Saunders et al., 1997; Jenkin et al., 2003; Saunders et al., 2003; Bloss et al., 2005a; Jenkin et al., 2015).

2.3 Meteorological and chemical conditions encountered during ICOZA

The overall conditions encountered during the ICOZA campaign are summarised by the time series of meteorological (wind
290   speed and direction, temperature, RH, photolysis frequencies) and chemical (mixing ratios of NO, NO_2, CO, HCHO, isoprene, MVK+MACR, O_3, HONO) parameters shown in Figure 2, which includes all available measurements at 15 min time resolution for the period 29th June – 22nd July 2015. As shown in Figure 3, the predominant wind sectors were W, SW, and S (i.e., ~180°– 270°). In terms of air mass back-trajectories (Cryer, 2016), during ICOZA the WAO site was generally under the influence of Atlantic air, which had been transported over the UK, likely encountering anthropogenic emissions from major conurbations
295   (e.g., Birmingham, London, Leicester; Figure 1). However, there were some exceptions to this on certain days of the campaign.

9

Atmospheric
Chemistry
and Physics
Discussions

For example, at the start of the campaign on 1st July, air that had spent a considerable amount of time over northern mainland Europe was sampled, which coincided with a heatwave (temperature of up to 30°C) and an event where high mixing ratios of ozone were encountered. Similarly, 11th and 16th July were characterised by a strong European influence, while on 9th July the site was subject to air masses originating from the North Sea.

300   During the ICOZA campaign, wind speeds were relatively strong, with a median of 5.5 m s^{-1} and a maximum of 12.7 m s^{-1}, and tended to drop slightly in the morning. Temperatures generally increased through the day from ~15°C before sunrise to ~20°C in the late afternoon, with a campaign maximum of 29.8°C during the heatwave on 1st July. RH varied between ~40–90% and was strongly anticorrelated with temperature. Based on Figure 3, and given that the SW sector corresponds to air that may have been transported over large urban areas (Figure 1), all ICOZA data (from 2nd July onwards) were split into two

305   categories according to wind direction – SW winds (180°–270°), and all other winds (NW–SE, <165° and >285°) – as shown in Table 2 and Figure 4. It can be seen that temperatures were generally higher (and conversely RH lower) in SW air. In addition, increased cloud cover in SW air is evident from the slightly lower average values of $J(O^1D)$.

        Overall, moderate levels of pollution were observed during the ICOZA campaign. For example, the campaign median NO mixing ratio, for periods of overlap with FAGE radical observations, was 160 pptv with a maximum of 4650 pptv (15 min).

310   NO generally peaked in the morning, with median values of ~500–1500 pptv at 08:00–10:00 Universal Time Coordinated (UTC = GMT = BST – 1), ~100–400 pptv in the afternoon, and <100 pptv at night (Figure 4). On average, NO mixing ratios were almost a factor of 2 higher in SW air than in NW–SE air (Table 2). NO$_2$ exhibited median and maximum levels of 2.2 and 10.4 ppbv, respectively, and followed an inverse diel profile to that of NO, peaking at night at ~3–4 ppbv with an afternoon minimum of ~1–1.5 ppbv. Both NO and NO$_2$ exhibited significant short-term variability (Figure 2).

315   The highest ozone mixing ratios of ~110 ppbv were observed on 1st July (Figure 2), which as mentioned above, coincided with elevated temperatures. It should be noted that this day, although interesting as a case study, was not characteristic of the general chemical conditions (particularly ozone levels) of the ICOZA campaign and was thus omitted from the wind sector analysis discussed in this paper (this includes Fig. 4 and Figs. 6–14); VOC measurements were also not available at this time. On average, ozone exhibits a classically-expected photochemical diel profile, with a minimum of ~25–30 ppbv around 06:00

320   UTC and a maximum of ~35–45 ppbv in the afternoon. Due to higher NO levels, O$_3$ mixing ratios were lower in SW air (Table 2).

        The diel profile of HCHO for SW air is similar to ozone (Figure 4), which is typical for an environment where HCHO production is largely driven by the photochemical oxidation of VOCs (Ayers et al., 1997; Cryer, 2016), with a diel minimum of ~800 pptv in the late morning and evening, and a maximum around 16:00 UTC in the range ~1000–1800 pptv. The diel

325   profile of HCHO in NW–SE air is less pronounced, with lower mixing ratios indicating less integrated photochemical processing. The highest HCHO levels of 3990 pptv were observed during the late morning of 4th July, although unfortunately radical and other measurements are not available for this time, owing to instrumental issues caused by a power cut on the preceding night.

Levels of HONO reached a maximum of ~570 pptv during the night that followed the daytime ozone event discussed
330   previously (1st–2nd July, Figure 2). In general, HONO mixing ratios tended to peak after sunset and midnight in NW–SE (~100
pptv) and SW air (~150 pptv), respectively. There is no obvious diel profile in CO measurements, and no clear difference
between NW–SE and SW wind, with median levels of ~90–150 ppbv observed throughout the day but a few short-term spikes
of up to ~420 ppbv. The flat diel profile observed for CO indicates that, for the most part, the WAO site was not strongly
impacted by fresh anthropogenic combustion emissions during the ICOZA campaign.

335   Isoprene levels were low during ICOZA, with a campaign median mixing ratio of 24 pptv and a maximum of 450 pptv.
Diel profiles of isoprene were similar between NW–SE and SW air, and bear slight resemblance to that expected from biogenic
emissions with a maximum of ~50 pptv in the afternoon/early evening. The isoprene oxidation products MVK and MACR,
measured as a sum using PTR–MS, exhibited significantly higher levels of ~80–200 pptv in SW air compared to ~20–60 pptv
in NW–SE air. $PM_{2.5}$ levels exhibited no clear diel profile, with similar loadings between the two wind sector types.

340   **3 Results**

3.1 Radical and OH reactivity observations and comparison to model predictions

Figure 5 shows the full time series of OH, HO_2, and total RO_2 radical concentrations as well as OH reactivity (15 min means)
observed during ICOZA, covering the period 29th June – 21st July 2015. Also shown are the MCM-base model results for all
radical species and k'_{OH} for periods in which measurements of all key species used to constrain the model were available, and
345   the PSS calculated OH concentrations. The radical observations follow their expected photochemical diel profiles, with
maximum levels around solar noon (~12:00 UTC on cloud-free days) and low nighttime concentrations, approximately an
order of magnitude smaller than during the daytime for OH and HO_2, and frequently scattered around zero. There was less of
a day-night contrast for total RO_2, for which nighttime levels were almost always above the RO_2 LOD (~5×10^7 molecule
cm^{-3} (~2 pptv)). Unlike radical concentrations, OH reactivity does not appear to show any diel pattern, with a median value of
350   4.7 s^{-1} but frequent spikes of up to ~10–15 s^{-1} (range = 1.7–17.6 s^{-1}). OH reactivity values were much higher at the start of the
campaign (i.e., 1st–2nd July 2015), due to the aforementioned heatwave event that coincided with the transport of pollution
from northern continental Europe (Cryer, 2016).

Daily maximum OH concentrations were in the range $2.6–17 \times 10^6$ molecule cm^{-3} and $1.8–13 \times 10^6$ molecule cm^{-3} for
observations and PSS calculations, respectively, based on the 90th percentile of the daytime concentrations with daytime
355   defined as $J(O^1D) > 5 \times 10^{-7}$ s^{-1}. The MCM-base modelled OH ($1.1–14 \times 10^6$ molecule cm^{-3}) is discussed in more detail
below. Similarly, daily maximum observed HO_2 and total RO_2 levels were in the range $0.75–4.2 \times 10^8$ molecule cm^{-3} and $2.3–$
8.0×10^8 molecule cm^{-3}, respectively, or $1.0–4.9 \times 10^8$ molecule cm^{-3} and $0.53–2.8 \times 10^8$ molecule cm^{-3} for MCM-base
predictions. It is clear from these features that the PSS calculation can broadly capture the range in daily maximum OH levels,
while the MCM-base model can generally reproduce peak HO_2 but significantly underpredicts midday total RO_2. Observed

11

360   nighttime concentrations were on the order of 1–3×10^5, 2–3×10^7, and 1–2×10^8 molecule cm^{-3} for OH, HO_2, and total RO_2, respectively (see Figure 6).

    On shorter timescales it can be seen (Figure 5) that the level of agreement is more variable. For example, the PSS calculation tracks OH observations very tightly for extended periods, but severe underpredictions are often found around midday, with smaller but still significant underpredictions on some mornings. The MCM-base predicted OH levels generally

365   follow changes in the measurements, but with a tendency towards overprediction during the daytime (median ~10%, see below). Similar to the PSS model capture of OH measurements, MCM-base modelled HO_2 concentrations show excellent agreement with measurements for much of the campaign (median daytime overprediction of ~3%). However, in contrast to the comparison between OH measurements and the PSS calculations, on other days the HO_2 observations were either under- or overpredicted, with roughly equal examples of each. For total RO_2 radicals, the level of agreement is poor (median daytime

370   underprediction of ~80%), where, with a few exceptions (e.g., 14th July), the MCM-base model cannot reproduce temporal changes in RO_2 concentrations, and generally cannot capture their magnitudes with any reasonable degree of success, consistent with the discrepancy between the predicted and observed ranges in daily maxima. OH reactivity is almost always underpredicted (daytime median ~35%), with a few examples of short periods where the MCM-base model reactivity matches the observations.

375   Figure 6 shows the median diel profiles of observed and modelled radical concentrations and OH reactivity, split by wind direction as in Figure 4. All radicals display their characteristic photochemical diel profiles, peaking around midday (albeit with strong day-to-day variability), and their qualitative features (i.e., overall shapes) are generally well-captured by the various model schemes. Smaller but still significant (i.e., above the LOD for each species) concentrations were observed at night that are generally larger than the model predictions.

380   Measured diel profiles of OH concentrations were similar in NW–SE and SW air, reaching ~2–4×10^6 molecule cm^{-3}, but with slight differences in the shape of their diel profiles. Overall, the models capture the observations reasonably well (i.e., generally within a factor of 2 during the daytime, although this is larger than the measurement uncertainty of 26% at 2σ), with the best agreement seen in SW air for the MCM-hox model (median difference ~15% during the daytime) and the PSS calculation (~20%). None of the models are able to capture the secondary maximum in OH levels in NW–SE air around 16:00

385   UTC. The PSS calculation underpredicts OH concentrations throughout the day in NW–SE air by ~35%, but tracks the measurements very tightly in SW air with a slight tendency towards underprediction. This suggests missing OH sources (see Equation (E2)), and is discussed in further detail in our companion paper (Woodward-Massey et al., 2022). For OH, differences between the MCM-base and MCM-carb models are only minor (median difference NW–SE ~1%, SW ~2%), with a greater difference seen for the MCM-hox run.

390   Measured HO_2 levels and diel profiles were very similar between the two wind sector types, with peak levels of around ~1–1.5×10^8 molecule cm^{-3} in the afternoon and nighttime concentrations on the order of ~2×10^7 molecule cm^{-3}. However, the MCM models predict very different behaviour in NW–SE and SW air. In NW–SE air, HO_2 levels are significantly underpredicted in the evening by a factor of ~2, but overpredicted by about a factor of ~2–3 in the afternoon. For SW air, HO_2

Atmospheric
Chemistry
and Physics
Discussions

Open Access
EGU

is still significantly underpredicted in the evening but agreement throughout the daytime is fairly reasonable (median ~1%
395   difference between measured HO_2 and MCM-carb), with less substantial afternoon disagreement. In either wind sector type,
there are strong differences, both positive and negative, between the MCM-base and MCM-carb models (range: −50% to
+70%).

Total RO_2 observations reached similar maximum concentrations of ~5×10^8 molecule cm^{-3} in NW–SE and SW air, but
exhibit different diel profiles. In NW–SE air, RO_2 levels peaked sharply just after midday, with concentrations of ~$1–3 \times 10^8$
400   molecule cm^{-3} in the morning and late afternoon. In SW air, the profile is broader, with concentrations of ~$2–4 \times 10^8$ molecule
cm^{-3} sustained from mid-morning to the afternoon and maximum levels observed around 16:00 UTC. In contrast to OH and
HO_2, the level of measurement/model agreement for total RO_2 is poor at all times of day, as might be expected based on their
time series comparison (Figure 5). For example, in NW–SE air, the measurement/MCM-base model ratios range from ~2–5 in
the afternoon to almost 40 in the early morning, with an average value of 8. Similar ratios are found in SW air, albeit with
405   more substantial afternoon disagreement, with an average of 9. The models do capture the general shape of the diel profiles,
not evident from the time series data in Figure 5, although, the models predict small secondary maxima in total RO_2 at night,
which is not seen in the measurements; such behaviour was also found in London (Whalley et al., 2018). Constraining the
model to the few measured carbonyls (MCM-carb) or HO_2 (MCM-hox) does little to improve the measurement-model
agreement.

410   OH reactivity exhibits similar behaviour in the two wind sector types, with relatively flat diel profiles and levels of 3–6
s^{-1}. In Figure 6, the grey dashed lines correspond to the OH reactivity from measured trace gases only, and the black lines are
the MCM-base model results that include contributions from model-generated intermediates (i.e., unconstrained OVOCs). In
NW–SE air, the model reactivity roughly tracks temporal changes in the measured reactivity (e.g., the afternoon decrease), but
the reactivity is underpredicted by ~34% throughout the day (maximum ~49%). The contribution of model intermediates to
415   model reactivity is ~35% on average, with an afternoon maximum of ~63%. In SW air, the measured OH reactivity profile is
flatter but is also underpredicted throughout the day by ~37% on average (maximum ~46%). Model intermediates were less
important than in NW–SE air, but accounted for a slightly greater proportion of model reactivity in the afternoon and evening
of up to ~30–40%, compared to ~22% on average.

3.2 RO₂ speciation

420   The RO_xLIF technique allows for "simple" (sRO_2) and "complex" (cRO_2) organic peroxy radicals to be measured separately,
as discussed in Section 2.1.1. RO_xLIF observations of speciated RO_2 radicals are compared to MCM-base model predictions
in Figure 7. On average, both observed and modelled sRO_2 account for ~60–100% of total RO_2 radicals. The overall levels of
sRO_2 (~$1–3 \times 10^8$ molecule cm^{-3}) and cRO_2 (~$0–1.5 \times 10^8$ molecule cm^{-3}) are similar between each wind sector type. In NW–
SE air, sRO_2 and cRO_2 display slightly different diel profile shapes, the latter being suppressed in the morning hours. sRO_2 are
425   always significantly underpredicted by the model (average measurement/model ratio ~ 9), whereas there is agreement for cRO_2
around ~06:00 and ~18:00 UTC but disagreement overall (average ratio ~ 7). In SW air, both diel profiles are broader and the

degree of underprediction in the afternoon is worse, with average values of ~10 and ~7 for sRO$_2$ and cRO$_2$, respectively. Similar to NW–SE air, agreement is also seen for cRO$_2$ in the early morning in SW air.

Figure 8 shows the daytime breakdown of RO$_2$ species predicted by the MCM-base model, split according to wind
430   direction. The model predicts that the dominant species in both wind sector types was methylperoxy (CH$_3$O$_2$), with contributions of ~58% and ~55% (daytime median) in NW–SE and SW air, respectively. In NW–SE air, the next most important species is HYPROPO2 (CH$_2$(OH)CH(CH$_3$)O$_2$, formed from OH addition to propene) with a contribution of ~9%, followed by acetylperoxy (CH$_3$CO$_3$, ~7%), BUTDBO2 (CH$_2$(OH)CH(O$_2$)CH=CH$_2$, formed from OH addition to 1,3-butadiene, ~2%), and HOCH2CH2O2 (CH$_2$(OH)CH$_2$O$_2$, formed from OH addition to ethene, ~2%). Other RO$_2$ radicals
435   contribute ~22% in total. In SW air, the contributions are fairly similar: HYPROPO2 ~6%, acetylperoxy ~8%, BUTDBO2 ~2%, and HOCH2CH2O2 ~2%. Other RO$_2$ radicals are slightly more important than in NW–SE air, with a total contribution of ~25%. Isoprene-derived peroxy radicals (with the most important being ISOPBO2 and ISOPDO2) contribute only ~2% and ~5% in NW–SE and SW air, respectively.

3.3 Observed and modelled OH vs $J(O^1D)$

440   Since OH is formed photochemically with ozone photolysis as a major source (Reaction (R1); see (Woodward-Massey et al., 2022)), OH levels are known to display a strong dependence on $J(O^1D)$. Strong correlations between OH and $J(O^1D)$ have been found for many field campaigns in a range of different environments (Ehhalt, 1999; Brauers et al., 2001; Creasey et al., 2003; Rohrer and Berresheim, 2006; Smith et al., 2006; Bloss et al., 2007; Emmerson et al., 2007; Smith, 2007; Furneaux, 2009; Lu et al., 2012; Vaughan et al., 2012; Lu et al., 2013; Tan et al., 2017; Tan et al., 2018b). In the present work, observed
445   and modelled OH concentrations are plotted against $J(O^1D)$ for NW–SE and SW air in Figure 9. Here, the data were split into 12 bins with the same number of points, to spread data evenly across the full range of $J(O^1D)$. Power law fits ($y = y0 + Ax^{pow}$) were applied to the datasets for comparison of fit parameters to previous work. The fit parameters may be interpreted as follows: (1) the intercept (y0) is a measure of OH production which does not require the presence of light, for example alkene ozonolysis (but which can also occur during the day); (2) the scaling factor (A) reflects the dependence of OH on other species
450   such as NO$_x$ and VOCs; (3) the power term (pow) represents the combined effects of photolytic processes (Rohrer and Berresheim, 2006). The fit parameters obtained are summarised in Table 3. In NW–SE air, measured OH concentrations exhibit an almost linear dependence on $J(O^1D)$, with a power term of 0.86. The fit to modelled OH exhibits more curvature, close to a square root dependence, and an intercept smaller than that for the measurements by a factor of 10. In SW air, the measured dependence is less linear (power term = 0.67) but the intercept is similar to that for NW–SE air. In contrast to NW–SE air, the
455   measurement and model curves are similar such that either can describe the data reasonably well. Overall, the power terms are amongst the lower values of previous reports, which ranged from 0.61–1.3 (Stone et al. (2012) and references therein). These power terms are most similar to those found for other coastal campaigns such as at Mace Head, Ireland (0.84; (Smith et al., 2006)) and Finokalia, Crete (0.68; (Berresheim et al., 2003)).

3.4 Observed and modelled RO_2 vs HO_2

460   It can be seen from Figure 5 and Figure 6 that RO_2 observations are well correlated with HO_2. To assess the strength of this correlation, RO_2 is plotted against HO_2 in Figure 10 for both measurement and model results, with fit parameters summarised in Table 4. Observed RO_2 and HO_2 are indeed strongly correlated, with a stronger correlation in SW air ($R = 0.81$ vs $R = 0.63$ in NW–SE air). For NW–SE air, the correlation is much stronger for sRO_2 vs HO_2 ($R = 0.68$) than cRO_2 vs HO_2 ($R = 0.37$) (data not shown). The fit slopes suggest that in NW–SE air RO_2 and HO_2 coexisted in approximately a 1:1 ratio, while this

465   was closer to 2:1 for SW air. The non-negligible intercepts of ~1–2 × 10^8 molecule cm^{-3} suggest that there are some RO_2 sources that do not result in the concomitant production of HO_2, consistent with the time series data in Figure 5, which may be more relevant at night and possibly indicates a contribution from NO_3 chemistry. For the model results, the $RO_2:HO_2$ ratio was closer to 1:2 in both NW–SE and SW air during the daytime, but much higher (~12:1) during nighttime. The different slopes for day and nighttime data in the model cases are not seen in the observations. The increased slope for the model results

470   during nighttime indicates slower $RO_2 \rightarrow HO_2$ cycling due to lower NO levels.

3.5 Observed and modelled OH, HO_2, RO_2, and k'_{OH} vs NO

Radical levels are known to display a strong dependence on NO_x concentrations since radical propagation is promoted by NO, and radical loss is often dominated by the reactions of radicals with NO and NO_2. In recent studies utilising the RO_xLIF technique, it has become apparent that measurement-model ratios for RO_2 are particularly sensitive to NO (Tan et al., 2017;

475   Tan et al., 2018b; Whalley et al., 2018; Slater et al., 2020; Whalley et al., 2020), which has implications for the calculation of ozone production rates, discussed in more detail in the companion to this paper (Woodward-Massey et al., 2022). The dependence of daytime ($J(O^1D) > 5 \times 10^{-7}\ s^{-1}$) radical concentrations and OH reactivity values on NO mixing ratios is shown in Figure 11, split according to wind direction. For OH only, both measured and modelled concentrations were normalised to the campaign-average $J(O^1D)$ to remove the dependence on OH source strength (= OH_Jnorm, e.g., (Tan et al., 2017)). This

480   approach is justified by the almost linear dependence of OH on $J(O^1D)$ (Figure 9); similar trends were also found for un-normalised OH albeit with more scatter (data not shown). The corresponding measurement-model ratios for radical species are shown in Figure 12.

     In NW–SE air, observed OH_Jnorm levels exhibit a classically-expected dependence on NO, increasing up to ~100 pptv NO before decreasing at higher NO (Figure 11). The MCM-base model reproduces the measured trend reasonably well.

485   However, the PSS model significantly underpredicts the observations at low NO, yielding measurement-model ratios of ~2–3 below ~200 pptv NO (Figure 12), which is greater than the estimated combined measurement-model uncertainty (~50%). In SW air, measured OH_Jnorm decreases with NO across the full NO range. The PSS model underpredicts the observations more severely at low NO (<300 pptv), yielding similar measurement-model ratios to those in NW–SE air. The MCM-base model slightly underpredicts the observations at low NO (by up to ~90%) but there is reasonable agreement (within ~40%) at

490   moderate to high NO (>300 pptv). The different behaviour for measured OH_Jnorm with respect to NO in NW–SE and SW

air might be expected from the strong differences in scaling factors (A, Figure 9 and Table 3) in the analysis in Section 3.3, which reflect the dependence of OH on species such as NO_x and VOCs.

Measured HO_2 in NW–SE air exhibits a weak decreasing trend with NO, with levels of ~0.7–1.3 × 10^8 molecule cm^{-3} below ~1 ppbv NO and ~0.3 × 10^8 molecule cm^{-3} above this threshold. In contrast, the model dependence on NO is much stronger such that HO_2 levels are overpredicted by up to a factor of ~3 at low NO. In the highest NO bin, measured HO_2 is underpredicted by a factor of ~2. In SW air, both measured and modelled HO_2 decrease sharply with NO, from ~2 × 10^8 molecule cm^{-3} at ~100 pptv NO to ~0.1–0.3 × 10^8 molecule cm^{-3} above 1 ppbv. For this wind direction, the measurements and model results are in agreement across the full NO range.

Overall, measured OH and HO_2 are in reasonable agreement with the PSS calculation and the MCM-base model prediction, respectively, at high NO. There is also good agreement between measured and MCM-base OH at moderate to high NO. However, RO_2 radicals are significantly underpredicted by the base model across all NO mixing ratios in both NW–SE and SW air. Observed and modelled RO_2 concentrations display a constant decrease with NO in either wind sector type. Comparing the two sets of observations, the dependence is steeper in SW air. In both wind sector types, the model NO dependence of RO_2 is steeper than the corresponding measurement NO dependence, such that the measurement-model ratio increases from ~2–3 for NO < 100 pptv to ~10–30 for NO > 1 ppbv (Figure 12). Such discrepancies likely relate to the model underprediction of OH reactivity, the degree of which also scaled with NO (Figure 11), since this indicates missing RO_2 sources from the OH oxidation of missing VOCs. Missing OH reactivity, i.e., the difference between measured and modelled OH reactivity, reached values of ~2–3 s^{-1} for NO > 1 ppbv, or ~30–45% of measured reactivity.

The increasing underprediction of RO_2 radicals as NO increases has been seen in all previous field campaigns in which RO_2 (distinct from HO_2) was measured using the RO_xLIF technique (Fuchs et al., 2008; Whalley et al., 2013). RO_2 measurement-model ratios as a function of NO from these campaigns (Tan et al., 2017; Tan et al., 2018b; Whalley et al., 2018; Slater et al., 2020; Whalley et al., 2020) are compared with ICOZA in Figure 13. It can be seen that the measurement-model discrepancy starts to appear at lower NO (i.e., <100 pptv) for ICOZA in comparison to the other campaigns, although the curves for ICOZA and AIRPRO summer display strong overlap in the ~100–600 pptv NO range. There is also some overlap between the curves for ICOZA and BEST-ONE (Tan et al., 2018b), a winter campaign conducted at a suburban site near Beijing, at low/moderate NO (~100–200 pptv). Overall, the largest measurement-model ratios were found in London (Whalley et al., 2018) and central Beijing (Slater et al., 2020; Whalley et al., 2020), but at higher NO levels (>10 ppbv) than those seen in most other campaigns including ICOZA.

To further explore the RO_2 discrepancy found for ICOZA, the contribution of sRO_2 to total RO_2 is plotted as a function of NO for measurement and model results in Figure 14. For the measurements, the sRO_2 contribution increases with NO in both NW–SE and SW air from ~0.7 to values close to 1. In contrast, the model predicts a constant sRO_2 fraction of ~0.7, in accordance with the dominance of CH_3O_2 (Figure 8). The reasons for the strong dependence of the measured sRO_2 fraction on NO are unclear, but may be due to the NO-mediated propagation of cRO_2 to sRO_2 as VOCs are increasingly fragmented into

smaller and less complex RO_2 species. Alternatively, cRO_2 formation may be facilitated by low NO_x levels, e.g., due to
525 autoxidation chemistry (Crounse et al., 2013; Jokinen et al., 2014; Bianchi et al., 2019).

3.6 Missing k'_{OH} vs OVOCs and temperature

Missing OH reactivity has been found in many previous field studies in which OH reactivity was measured and compared to
calculated reactivity or model simulations (Kovacs et al., 2003; Ren et al., 2003; Di Carlo et al., 2004; Sinha et al., 2008; Lee
et al., 2009b; Lou et al., 2010; Mao et al., 2012; Nolscher et al., 2012; Edwards et al., 2013; Brune et al., 2016; Whalley et al.,
530 2016; Kumar et al., 2018). Missing OH reactivity is normally attributed to either unmeasured primary VOCs (e.g., BVOCs),
or unmeasured VOC oxidation products (i.e., OVOCs). To test which was responsible for the missing reactivity observed for
ICOZA, missing OH reactivity (measured – modelled) was binned against various chemical concentrations and temperature.
These data are shown in Figure 15. It can be seen that missing reactivity exhibits strong correlations ($R^2 \geq 0.83$) with several
measured OVOCs, such as acetaldehyde, acetone, and methanol (all constrained in MCM-base). This finding suggests that the
535 missing reactivity is due to unmeasured VOC oxidation products that were not well simulated by the base model. The only
OVOCs measured and constrained in the base model were acetone, acetaldehyde, and methanol and as such many OVOCs
were missing, e.g., the oxidation products of $>C_2$ VOCs. Weaker correlations ($R^2 \leq 0.7$) were found for isoprene (maximum =
418 pptv) and the PTR-MS measured sum of monoterpenes (maximum = 105 pptv), such that unmeasured primary BVOCs
are unlikely to be the root of the missing reactivity. BVOC emissions are known to display an exponential dependence on
540 temperature (Guenther et al., 1993). It is therefore expected that missing reactivity should scale exponentially with temperature
if missing biogenic species are responsible (Di Carlo et al., 2004). As shown in Figure 15, this was not the case for ICOZA
and the dependence is clearly linear, albeit over a relatively small temperature range of ~12–24°C. This is further evidence
that the missing reactivity for ICOZA is due to OVOCs, not a primary biogenic species. It is hypothesised that the correlation
with temperature is due to increased VOC oxidation rates at high temperature that results in greater OVOC production. Missing
545 reactivity is also reasonably well correlated with toluene ($R^2 = 0.84$, data not shown), such that unmeasured aromatic VOCs
could also be responsible, as suggested by Lee et al. (2009b).

When missing OH reactivity is calculated using the MCM-carb model, which is additionally constrained to measured
HCHO and MVK+MACR, all the correlations in Figure 15 remain ($R^2 \geq 0.83$), with the exception of temperature ($R^2 = 0.61$).
Therefore, species other than HCHO and MVK+MACR must be responsible for the missing OH reactivity. In recent years,
550 OVOC emissions have increased in importance in the UK, with ethanol now the largest contributor to non-methane VOCs in
terms of mass emissions (Lewis et al., 2020). More generally, alcohols are now the largest contributors to ozone production
(~30%) in terms of their photochemical ozone creation potentials (POCPs). It is therefore critical that in future field campaigns,
alcohols such as ethanol and isopropanol are measured to evaluate their impacts on radical budgets and ozone production.

4 Discussion

555 ### 4.1 Comparison to previous coastal field campaigns

OH, HO_2, and OH reactivity have previously been measured at the WAO using FAGE, most recently in May 2004 as part of the TORCH 2 campaign (Smith, 2007; Lee et al., 2009b). However, NO levels were generally higher during TORCH-2 (mean 0.62 ppbv, range ~0–50 ppbv) than ICOZA (mean 0.38 ppbv, range ~0–7.5 ppbv), likely due to NO_x emissions reductions over the 11 years that separate the two campaigns (https://www.gov.uk/government/statistics/emissions-of-air-

560 pollutants/emissions-of-air-pollutants-in-the-uk-nitrogen-oxides-nox). On a diel-average basis, OH peaked at 12:00 UTC with similar levels (~4×10^6 molecule cm^{-3}) to ICOZA. OH has also been measured by DOAS at the WAO, with measured peak daytime levels of ~4–7×10^6 molecule cm^{-3} (Forberich et al., 1999; Grenfell et al., 1999). For other ground and ship-based campaigns in the MBL, measured noontime OH concentrations were mostly in the range ~4–6×10^6 molecule cm^{-3}, and generally the observations have been found to agree with model predictions to within ~30% on average during the daytime in

565 the MBL (Sommariva et al., 2004; Sommariva et al., 2006; Whalley et al., 2010; Beygi et al., 2011; Van Stratum et al., 2012). During the NASA airborne Atmospheric Tomography study (ATom), OH concentrations in the MBL were on the order of ~1–4×10^6 molecule cm^{-3} and a model was able to reproduce them to generally within 40% (Brune et al., 2020).

Measured HO_2 levels were also very similar during TORCH 2, peaking in the afternoon (~14:00 UTC) at ~8×10^7 molecule cm^{-3} (cf. 1×10^8 molecule cm^{-3} for ICOZA, Figure 6) (Smith, 2007). For other previous measurements of HO_2, the

570 observed concentrations and levels of measurement-model agreement have generally been quite variable. In terms of HO_2, ICOZA is most similar to the North Atlantic Marine Boundary Layer EXperiment (NAMBLEX), which took place at Mace Head, Ireland, in summer 2002 (Heard et al., 2006). During NAMBLEX, noontime HO_2 concentrations were in the range 0.9–2.1×10^8 molecule cm^{-3} and were overpredicted by up to a factor of 2 (Sommariva et al., 2006). These results are almost identical to the findings of ICOZA despite the substantial differences in chemical conditions (e.g., the much lower

575 anthropogenic influence and the role of halogen species during NAMBLEX). During the Diel Oxidants Mechanisms In relation to Nitrogen Oxides (DOMINO) campaign in SW Spain in Nov–Dec 2008 (Van Stratum et al., 2012), similar HO_2 levels of up to ~1.5×10^8 molecule cm^{-3} were observed (in continental air, analogous to the SW sector in the present work). However, model calculations were only performed for one day, using a mixed layer model, which showed significant morning and afternoon underpredictions. This may be due in part to interferences from RO_2 radicals (Fuchs et al., 2011; Whalley et al.,

580 2013), which were not known about at the time. For other campaigns, HO_2 concentrations were generally above ~2×10^8 molecule cm^{-3} (Sommariva et al., 2004; Whalley et al., 2010; Beygi et al., 2011), higher than the range observed during ICOZA (~0.5–2×10^8 molecule cm^{-3}), and the observations have mostly been overpredicted. During ATom, HO_2 concentrations in the MBL were on the order of ~1–5×10^8 molecule cm^{-3} and were well captured by a model (agreement within 40%) (Brune et al., 2020).

585 RO_2 radicals were not measured during TORCH 2, but the sum of peroxy radicals ($HO_2 + RO_2$) have been measured using peroxy radical chemical amplification (PERCA) during other campaigns at the WAO (Penkett et al., 1999; Fleming et al.,

2006; Green et al., 2006). The most recent campaign, INSPECTRO (Influence of clouds on the spectral actinic flux in the lower troposphere), took place in September 2002 (Green et al., 2006). Peak $HO_2 + RO_2$ levels of ~2–5 $\times 10^8$ molecule cm^{-3} were observed at or a few hours after solar noon, with nighttime levels on the order of ~5–7 $\times 10^7$ molecule cm^{-3}. In

590 comparison, $HO_2 + RO_2$ concentrations during ICOZA were fairly similar during the daytime with levels of ~4–6 $\times 10^8$ molecule cm^{-3} at solar noon (Figure 6), but nighttime concentrations were approximately 3–4 times higher (~2 $\times 10^8$ molecule cm^{-3}). It is possible that during ICOZA, nighttime ozonolysis or NO_3 radical chemistry was more active. Nighttime $HO_2 + RO_2$ levels of up to ~1 $\times 10^8$ molecule cm^{-3} were observed using PERCA at Mace Head during the Eastern Atlantic Spring Experiment (EASE 97) in April–May 1997 (Salisbury et al., 2001). During DOMINO 2008, which was heavily influenced by

595 urban-industrial/petrochemical emissions, $HO_2 + RO_2$ concentrations measured by PERCA were much higher, with daytime maxima of ~2–12 $\times 10^8$ molecule cm^{-3} and frequent nighttime spikes of up to ~20 $\times 10^8$ molecule cm^{-3} on nights with air arriving from the industrial sector (Andres-Hernandez et al., 2013). Similarly, during TexAQS (Texas Air Quality Study) 2006, ship-based PERCA measurements in industrial regions around Houston, Texas showed that $HO_2 + RO_2$ levels could reach ~30 $\times 10^8$ molecule cm^{-3} during nighttime (Sommariva et al., 2011) in highly polluted areas, although, in less polluted areas,

600 nighttime $HO_2 + RO_2$ levels were on the order ~2–10 $\times 10^8$ molecule cm^{-3}.

      The mean OH reactivity measured during TORCH 2 (4.9 s^{-1}) is virtually identical to that measured during ICOZA (5.0 s^{-1}) (Lee et al., 2009b). The maximum OH reactivity was higher for ICOZA (17.6 s^{-1}) than TORCH 2 (9.7 s^{-1}) due to the pollution episode at the start of ICOZA (Figure 2). The mean missing OH reactivity in terms of the difference between measured OH reactivity and that calculated using trace gases only was 1.9 s^{-1} (39%) during TORCH 2 (cf. 2.4 s^{-1}, 48% for

605 ICOZA). A box model using MCMv3.1 chemistry (Bloss et al., 2005a) was used to simulate OH reactivity, reducing the missing reactivity to 1.4 s^{-1} or 29% (cf. 1.7 s^{-1}, 36% for ICOZA). Lee et al. (2009b) speculated that the missing reactivity may be due to a potentially large number of unmeasured, high molecular weight aromatic compounds, but that this could also be due to missing OVOCs, as we have suggested based on the data in Figure 15. OH reactivity was measured using the comparative reactivity method (CRM) at a Mediterranean coastal receptor site in Corsica, France during summer 2013

610 (Zannoni et al., 2017). Total OH reactivity reached a maximum of ~17 s^{-1} with an average of ~5 s^{-1}, where 44% of the reactivity was missing. OH reactivity was much higher during the DOMINO campaign due to the influence of urban-industrial/petrochemical emissions, with an average value of 18 s^{-1} measured using the CRM (Sinha et al., 2012).

      To date, only a handful of studies have measured OH reactivity at coastal locations but there have been airborne campaigns conducted in the marine boundary layer. An airborne OH reactivity instrument was deployed during flights over the Pacific

615 Ocean for the Intercontinental Chemical Transport Experiment-B (INTEX-B) campaign (Mao et al., 2009). In the boundary layer (i.e., < 2 km altitude), measured OH reactivity was ~4 s^{-1} on average, while that calculated from measured reactants was only ~1.5–2 s^{-1} (i.e., ~50–60% missing), similar to ICOZA. During the NASA Atmospheric Tomography (ATom) campaign involving flights over the Atlantic and Pacific Oceans, measured OH reactivity at < 2 km was on the order of ~2 s^{-1}, with missing reactivity on the order of ~0.5–1 s^{-1} (~25–50% missing) (Thames et al., 2020). The authors suggested that, based on

620   correlations of missing OH reactivity with HCHO, DMS, butanal, and sea surface temperature, there were unmeasured/unknown VOCs/OVOCs associated with oceanic emissions, in agreement with our findings.

4.2 Differences and similarities between the NW–SE and SW wind sectors

Differences between the NW–SE and SW wind sectors in terms of radical and OH reactivity levels, and model performance, were expected based on the strong differences in chemical conditions between the two wind sector types (Table

625   2 and Figure 4). However, many aspects are fairly similar between the two wind sector types, for example measured OH, HO_2, RO_2, and OH reactivity levels. Perhaps the most striking difference between the two wind sector types is the model performance for OH and HO_2 (Figure 6). In NW–SE air, measured OH is underpredicted by the PSS calculation by ~35% on average, but reasonable agreement is found in SW air (within 20% on average). Similarly, HO_2 is overpredicted by both the MCM-base and MCM-carb models by a factor of 2–3 during the afternoon in NW–SE air, but reasonable agreement is found

630   between measured HO_2 and the MCM-carb model for daytime SW air. In contrast, the model underprediction of RO_2 is more severe in SW air compared to the NW–SE sector, suggesting that the good agreement found for HO_2 may be fortuitous (i.e., if the model was able to reproduce RO_2, then $RO_2 + NO \rightarrow HO_2$ reactions would likely lead to the model overpredicting HO_2). The underprediction of OH and overprediction of HO_2 in NW–SE air, only occurs at low-NO_x (Figure 11 and Figure 12). Possible reasons for these discrepancies are discussed in Section 4.4.

635   ### 4.3 Differences between models

The carbonyls HCHO and MVK+MACR were not constrained in the MCM-base model because of several gaps in the time series of these measurements. The MCM-base model performance in simulating these carbonyls was assessed, where it was found that there was reasonable agreement for MVK+MACR on a diel average basis, but that HCHO concentrations were significantly overpredicted in the afternoon (data not shown). The differences in the calculated concentrations of these OVOC

640   compounds is the cause of the differences between the MCM-base and MCM-carb simulations of radical species (Figure 6). Similarly, HO_2 concentrations were generally overpredicted by both the MCM-base and MCM-carb models, and therefore constraining to HO_2 (MCM-hox model) has impacts on the model OH and RO_2 concentrations (Figure 6). Since the MCM-base model also underpredicted OH reactivity, there are additional differences between the PSS calculation of OH and the MCM model predictions.

645   For OH, differences between the MCM-base and MCM-carb runs are relatively minor and both positive and negative (Figure 6). There are two competing effects here: HCHO is a minor OH sink (~6% (Woodward-Massey et al., 2022)) and thus an overprediction of HCHO would lead to lower OH in MCM-base relative to MCM-carb. In contrast, the base model overprediction of HCHO leads to a greater HO_2 source strength that would drive higher OH levels in MCM-base relative to MCM-carb. Similarly, HO_2 was overpredicted in MCM-base and MCM-carb such that constraining the model to HO_2 (MCM-

650   hox) resulted in lower model OH levels. Finally, due to the MCM model underprediction of OH reactivity, PSS calculated OH levels were lower than the MCM model concentrations. At low NO (Figure 11), the better agreement found for the OH/MCM-

base case compared to the OH/PSS case is driven by the MCM overprediction of HO_2, i.e., the agreement for OH does not necessarily mean the OH chemistry is well understood at low NO. Peak afternoon RO_2 concentrations were similar for the MCM-base and MCM-carb simulations (Figure 6). However, the reduced OH in MCM-hox results in reduced afternoon RO_2

655   levels.

4.4 Overprediction of HO_2 under low-NO_x conditions in NW–SE air

In several previous field campaigns, HO_2 concentrations were overpredicted under low-NO_x conditions (Sommariva et al., 2004; Sommariva et al., 2006; Kanaya et al., 2007; Griffith et al., 2013; Whalley et al., 2018). Extremely low NO levels of < 3 pptv were observed during the Southern Ocean Photochemistry Experiment (SOAPEX-2), which took place at Cape Grim

660   in austral summer 1999. HO_2 observations were overpredicted by ~40%, but improved agreement could be found by inclusion of HO_2 uptake with an uptake coefficient (γ_{HO2}) of unity (Sommariva et al., 2004). HO_2 uptake was considered in the present work, using $\gamma_{HO2} = 0.1$. In our companion paper, we show that even increasing γ_{HO2} to unity has little impact on the experimental budget for HO_2, thus heterogeneous uptake alone cannot explain the HO_2 measurement-model discrepancy under low-NO_x conditions in NW–SE air during ICOZA.

665   As discussed above, HO_2 measurements were overpredicted by a factor of 2 during NAMBLEX, for which the model analysis was performed for days with low NO_x levels (NO < 30 pptv) (Sommariva et al., 2006). Agreement was improved when the model was constrained to measured OVOCs (acetaldehyde, methanol, and acetone in the case of NAMBLEX), similar to the improvement in measurement-model agreement seen for the MCM-carb run (constrained to HCHO and MVK+MACR) in the present work (Figure 6). Additionally, at Mace Head, seaweed beds are exposed at low tide that represent

670   a significant source of reactive halogen species such as I_2 and CH_2I_2 (Carpenter et al., 1999; Carpenter et al., 2003; Mcfiggans et al., 2004). Halogen oxides (XO, where X = Br, I) are able to convert HO_2 to OH:

$$HO_2 + XO \rightarrow HOX + O_2 \tag{R7}$$

$$HOX + h\nu \rightarrow OH + X, \tag{R8}$$

where hypohalous acids (HOX) may also undergo heterogeneous loss to aerosols. In a steady-state analysis, (Bloss et al.,

675   2005b) found that up to 40% of HO_2 could be lost to IO under low-NO_x conditions, for measured IO levels of 0.8–4.0 pptv (Commane et al., 2011). In the full modelling study (Sommariva et al., 2006), constraining the model to BrO and IO resulted in similar decreases in model HO_2, depending on the uptake coefficients used for HOI and HOBr. Reactive iodine species were not measured during ICOZA, and their influence is expected to be negligible due to the lack of seaweed beds at the WAO site. However, it is possible that there was a source of reactive bromine through sea salt aerosol chemistry (Keene et al., 2009). We

680   therefore speculate that inclusion of reactive halogens could simultaneously reduce the underprediction of OH and the overprediction of HO_2 under low-NO_x conditions in NW–SE air. To our knowledge there have been no measurements of I_2, BrO, or IO at the WAO (John Plane, personal communication). In our companion paper (Woodward-Massey et al., 2022), we show that incorporation of an artificial species "Y" that converts HO_2 to OH (Lu et al., 2012; Lu et al., 2013) does result in slight improvements to the agreement between experimental OH and HO_2 production and destruction rates. We also speculate

21

685   that if another artificial species "Z" is able to convert HO_2 to RO_2, this would reduce both the overprediction of HO_2 and the underprediction of RO_2 at low-NO_x conditions (Figure 11 and Figure 12 in the present work).

OH and HO_2 were measured at Rishiri Island, Japan, in September 2003 (Kanaya et al., 2007). Daytime HO_2 levels were overpredicted by almost a factor of 2. In addition to halogen chemistry and HO_2 uptake, the authors also considered the possibility that $HO_2 + RO_2$ reactions were faster than previously thought. In our companion paper, we show that RO_2

690   destruction rates exceed RO_2 production rates at high NO, but the two are equal at low NO. Increasing the rate of $HO_2 + RO_2$ reactions would result in increased RO_2 destruction rates, therefore worsening the agreement between RO_2 destruction and production rates, which should be in balance. For this reason, we do not think that faster-than-expected $HO_2 + RO_2$ reactions are the cause of the overprediction of HO_2 levels under low-NO_x conditions in NW–SE air during ICOZA.

During the Clean air for London (ClearfLo) campaign in summer 2012, HO_2 concentrations were overpredicted by a box

695   model using MCMv3.2 by up to a factor of 10 at low NO (< 1 ppbv) (Whalley et al., 2018). The model HO_2 was somewhat reduced but the observations could still not be reconciled after inclusion of both HO_2 aerosol uptake (using $\gamma_{HO_2} = 1$) and autoxidation chemistry (Bianchi et al., 2019), which is now known to play a significant role in the gas phase oxidation of both BVOCs (Crounse et al., 2011; Ehn et al., 2014; Jokinen et al., 2014; Berndt et al., 2016; Zha et al., 2017) and anthropogenic VOCs (AVOCs) (Wang et al., 2017; Molteni et al., 2018; Mehra et al., 2020; Wang et al., 2020). Whalley et al. (2018) found

700   that good agreement between the model and HO_2 measurements could be found if the rate of $RO_2 + NO \rightarrow HO_2$ propagation was reduced, in their case by reducing the branching ratio for alkyl nitrate formation. In our companion paper, we show that reducing the rate of $RO_2 + NO \rightarrow HO_2$ propagation does help to resolve budget imbalances for HO_2 and RO_2, even at the lower NO levels observed in the afternoon due to the dominance of $RO_2 + NO$ as an RO_2 sink and HO_2 source.

4.5 Underprediction of RO_2 under high-NO_x conditions

705   Under moderate and high-NO_x conditions (above ~200–300 pptv NO), reasonable measurement-model agreement is found for OH and HO_2, i.e., generally to within a factor of 2 (Figure 11 and Figure 12). However, total RO_2 concentrations are much more significantly underpredicted, by as much as a factor of ~30 at the highest NO levels encountered (above ~2 ppbv), coincident with increased missing OH reactivity. As shown in Figure 13, this phenomenon has been observed in several other field campaigns (Tan et al., 2017; Tan et al., 2018b; Whalley et al., 2018; Slater et al., 2020; Whalley et al., 2020). Tan et al.

710   (2017) found that an additional primary RO_2 source from chlorine chemistry could explain a small portion (10–20%) of the missing RO_2 in their study. Whalley et al. (2018) found that chlorine chemistry increased modelled RO_2 for the ClearfLo campaign by ~20% in the morning when NO_x levels were high, in comparison to RO_2 underpredictions of greater than factor of 10. Since the major Cl atom precursor $ClNO_2$ was measured during ICOZA (Sommariva et al., 2018) and constrained in all model scenarios, $ClNO_2$ photolysis to form Cl atoms and the subsequent reactions of Cl with VOCs is not thought to be the

715   source of the missing RO_2 in the present study. However, as the chlorine chemistry in MCMv3.3.1 is limited to reactions with alkanes, additional chlorine chemistry (e.g., reactions with alkenes, OVOCs, etc.) may be needed to fully assess the role of chlorine during ICOZA.

Atmospheric
Chemistry
and Physics
Discussions

Since missing OH reactivity was also found at high NO_x conditions, some of the missing RO_2 may be due to the reactions of OH with unmeasured VOCs. However, as we show in our companion paper (Woodward-Massey et al., 2022), evidence is

720 also found for missing RO_2 sources at high NO_x using calculations constrained to measured OH reactivity. Thus the missing OH reactivity cannot fully explain the missing RO_2. It is possible that the missing RO_2 found for ICOZA is not due to a missing RO_2 source, but an overestimated RO_2 sink. As discussed above, reducing the rate of $RO_2 + NO \rightarrow HO_2$ propagation (i.e., a reduced RO_2 sink) helps to resolve budget imbalances for HO_2 and RO_2, similar to that found for HO_2 by Whalley et al. (2018). We found the largest improvement to the experimental budget balance in the morning, when NO_x levels were at their highest.

725 However, the $RO_2 + NO$ rate constant (originally the generic value used in the MCM) had to be reduced by a factor of 5, when laboratory measurements of such rate constants have not reported values as low and have uncertainties in the range ~15–35% (Orlando and Tyndall, 2012).

Recently, Whalley et al. (2020) presented measurements of OH, HO_2, RO_2, and OH reactivity in summertime Beijing. RO_2 concentrations were underpredicted by a box model with MCMv3.3.1 chemistry, most severely at high NO_x (Figure 13).

730 Missing OH reactivity was also identified. The measurement-model agreement for RO_2 was significantly improved after the model inclusion of an α-pinene derived RO_2 radical, C96O2 (MCM nomenclature), formed at a rate set equal to the level of missing OH reactivity. This complex RO_2 species does not generate HO_2 directly from its reaction with NO, but instead the RO radical formed preferentially isomerises (via a H-shift) to form another RO_2 radical in the presence of O_2, and undergoes multiple $RO_2 + NO \rightarrow R'O_2$ reactions before eventually forming HO_2. Such autoxidation chemistry has the net effect of

735 reducing the rate of $RO_2 \rightarrow HO_2$ propagation, and effectively extends the lifetime of RO_2 radicals, resulting in higher concentrations. Based on the results in the present work, it is possible that similar chemistry occurred during the ICOZA campaign, although it is unlikely that a BVOC was involved because of the low biogenic influence at the WAO site. However, aromatic species, more relevant to ICOZA, have also been shown to undergo autoxidation (Wang et al., 2017; Mehra et al., 2020).

740 **5 Conclusions**

OH, HO_2, and RO_2 radicals and OH reactivity (k'_{OH}) were measured at a UK coastal receptor site during the July 2015 ICOZA intensive field campaign. Maximum measured daily OH, HO_2, and total RO_2 radical concentrations were in the range 2.6–17 $\times 10^6$, 0.75–4.2 $\times 10^8$, and 2.3–8.0 $\times 10^8$ molecule cm^{-3}, respectively. k'_{OH} ranged from 1.7 to 17.6 s^{-1} with a median value of 4.7 s^{-1}. ICOZA data were split by wind direction to assess differences in the radical chemistry between air that had passed over

745 the North Sea (NW–SE sectors) or over major urban conurbations such as London (SW sector). A PSS calculation underpredicted daytime OH in NW–SE air by ~35% on average, whereas agreement was found within instrumental uncertainty (~26% at 2σ) in SW air. The OH levels predicted by a box model using MCM chemistry were in better agreement with the measurements. However, for HO_2, the base MCM model overpredicted the observations in NW–SE air in the afternoon by a factor of ~2–3, whereas reasonable agreement was found for HO_2 in SW air when the model was constrained to measured

750   carbonyls (HCHO, MVK+MACR). In contrast, for total RO_2, the model severely underpredicted the observations in both NW–SE and SW air, with measurement/model ratios ranging from ~2–5 in the afternoon to almost 40 in the early morning. The model predicted that the dominant RO_2 species in both wind sector types was CH_3O_2. k'_{OH} observations were underpredicted by ~34% and ~37% in NW–SE and SW air, respectively.

    Measured OH levels were well correlated with $J(O^1D)$, where power law fits to measured OH vs $J(O^1D)$ yielded power

755   terms similar to previous coastal field campaigns. Good correlations were also observed between measured total RO_2 and measured HO_2, and the fit slopes indicated that the RO_2:HO_2 ratio was close to 1:1 in NW–SE air and ~2:1 in the more polluted SW air. The slopes of modelled RO_2 vs modelled HO_2 were different between day and nighttime data, which was not seen in the observations.

    Measured radical and k'_{OH} levels and measurement-to-model ratios displayed strong dependences on NO mixing ratios.

760   For OH, the PSS calculation could capture the observations at high NO (> 1 ppbv), but underpredicted the observations at low NO (< 200–300 pptv) by a factor of ~2–3, suggesting missing OH sources. The MCM-base model performed better in terms of reproducing the observed dependence of OH on NO but there was still a tendency towards underprediction at low NO. The MCM-base model overpredicted HO_2 concentrations at low NO in NW–SE air by a factor of ~3, whereas in SW air, the measurements and model results were in agreement across the full NO range. For RO_2, measurement-to-model ratios scaled

765   with NO, from ~2–3 for NO < 100 pptv to ~10–30 for NO > 1 ppbv, a trend found in all previous field campaigns in which RO_2 was measured using the RO_xLIF technique. This suggests that peroxy radical chemistry is not well understood under high NO_x conditions. Missing OH reactivity, i.e., the difference between measured and modelled k'_{OH}, also scaled with NO. The strong correlation of missing OH reactivity with several OVOCs suggests that the missing reactivity was due to unmeasured VOC oxidation products that were not well simulated by the model, rather than a primary VOC species (e.g., a BVOC).

770   In our companion paper (Woodward-Massey et al., 2022), we analyse the experimental radical budgets, which are derived from measured quantities only (Tan et al., 2018a), and discuss the main sources and sinks of total RO_x and OH radicals. In addition, we calculate *in situ* ozone production rates from our measurements of peroxy radicals and compare them to those predicted by the MCM model.

Data availability

775   The data used in this study are available from the corresponding authors upon request (l.k.whalley@leeds.ac.uk and d.e.heard@leeds.ac.uk) and are also archived on CEDA (https://archive.ceda.ac.uk/).

Author contributions

    WJB was the principal investigator of the ICOZA project and was responsible for organisation of the Weybourne field intensive. RWM, LKW, DRC, TI, and DEH were responsible for measurements of radicals, OH reactivity, HCHO, and

Atmospheric
Chemistry
and Physics
Discussions

780   photolysis frequencies (*J* values also provided by RS and PSM). LRC, LJK, and WJB made measurements of HONO and aerosol surface area. JL and CR measured NO, NO$_2$, and HONO. BJB was responsible for the long-term operation of the Weybourne Atmospheric Observatory and provided O$_3$, CO, and HCHO data. GLF was responsible for measurements of VOCs. RS and SC developed the AtChem modelling framework. RS conducted the MCM model simulations. RWM, LKW, and RS analysed the data. RWM wrote the manuscript with input from all co-authors.

References

795   Andres-Hernandez, M. D., Kartal, D., Crowley, J. N., Sinha, V., Regelin, E., Martinez-Harder, M., Nenakhov, V., Williams, J., Harder, H., Bozem, H., Song, W., Thieser, J., Tang, M. J., Beigi, Z. H., and Burrows, J. P.: Diel peroxy radicals in a semi-industrial coastal area: nighttime formation of free radicals, Atmos Chem Phys, 13, 5731-5749, 10.5194/acp-13-5731-2013, 2013.

Ayers, G. P., Gillett, R. W., Granek, H., de Serves, C., and Cox, R. A.: Formaldehyde production in clean marine air, Geophys
800   Res Lett, 24, 401-404, 10.1029/97gl00123, 1997.

Berndt, T., Richters, S., Jokinen, T., Hyttinen, N., Kurten, T., Otkjaer, R. V., Kjaergaard, H. G., Stratmann, F., Herrmann, H., Sipila, M., Kulmala, M., and Ehn, M.: Hydroxyl radical-induced formation of highly oxidized organic compounds, Nat Commun, 7, 13677, 10.1038/ncomms13677, 2016.

Berresheim, H., Plass-Dülmer, C., Elste, T., Mihalopoulos, N., and Rohrer, F.: OH in the coastal boundary layer of Crete
805   during MINOS: Measurements and relationship with ozone photolysis, Atmos. Chem. Phys., 3, 639-649, 10.5194/acp-3-639-2003, 2003.

Beygi, Z. H., Fischer, H., Harder, H. D., Martinez, M., Sander, R., Williams, J., Brookes, D. M., Monks, P. S., and Lelieveld, J.: Oxidation photochemistry in the Southern Atlantic boundary layer: unexpected deviations of photochemical steady state, Atmos Chem Phys, 11, 8497-8513, 10.5194/acp-11-8497-2011, 2011.

810   Bianchi, F., Kurtén, T., Riva, M., Mohr, C., Rissanen, M. P., Roldin, P., Berndt, T., Crounse, J. D., Wennberg, P. O., Mentel, T. F., Wildt, J., Junninen, H., Jokinen, T., Kulmala, M., Worsnop, D. R., Thornton, J. A., Donahue, N., Kjaergaard, H. G., and Ehn, M.: Highly Oxygenated Organic Molecules (HOM) from Gas-Phase Autoxidation Involving Peroxy Radicals: A Key Contributor to Atmospheric Aerosol, Chemical Reviews, 119, 3472-3509, 10.1021/acs.chemrev.8b00395, 2019.

Bloss, C., Wagner, V., Jenkin, M. E., Volkamer, R., Bloss, W. J., Lee, J. D., Heard, D. E., Wirtz, K., Martin-Reviejo, M., Rea,
815   G., Wenger, J. C., and Pilling, M. J.: Development of a detailed chemical mechanism (MCMv3.1) for the atmospheric oxidation of aromatic hydrocarbons, Atmos Chem Phys, 5, 641-664, DOI 10.5194/acp-5-641-2005, 2005a.

Bloss, W. J., Lee, J. D., Heard, D. E., Salmon, R. A., Bauguitte, S. J. B., Roscoe, H. K., and Jones, A. E.: Observations of OH and HO_2 radicals in coastal Antarctica, Atmos Chem Phys, 7, 4171-4185, DOI 10.5194/acp-7-4171-2007, 2007.

Bloss, W. J., Lee, J. D., Johnson, G. P., Sommariva, R., Heard, D. E., Saiz-Lopez, A., Plane, J. M. C., McFiggans, G., Coe,
820   H., Flynn, M., Williams, P., Rickard, A. R., and Fleming, Z. L.: Impact of halogen monoxide chemistry upon boundary layer OH and HO_2 concentrations at a coastal site, Geophys Res Lett, 32, L06814, Artn L06814 10.1029/2004gl022084, 2005b.

Bohn, B., Corlett, G. K., Gillmann, M., Sanghavi, S., Stange, G., Tensing, E., Vrekoussis, M., Bloss, W. J., Clapp, L. J., Kortner, M., Dorn, H. P., Monks, P. S., Platt, U., Plass-Dulmer, C., Mihalopoulos, N., Heard, D. E., Clemitshaw, K. C.,
825   Meixner, F. X., Prevot, A. S. H., and Schmitt, R.: Photolysis frequency measurement techniques: results of a comparison within the ACCENT project, Atmos Chem Phys, 8, 5373-5391, DOI 10.5194/acp-8-5373-2008, 2008.

Bohn, B., Heard, D. E., Mihalopoulos, N., Plass-Dülmer, C., Schmitt, R., and Whalley, L. K.: Characterisation and improvement of $j(O^1D)$ filter radiometers, Atmos Meas Tech, 9, 3455-3466, 10.5194/amt-9-3455-2016, 2016.

830   Brauers, T., Hausmann, M., Bister, A., Kraus, A., and Dorn, H. P.: OH radicals in the boundary layer of the Atlantic Ocean 1. Measurements by long-path laser absorption spectroscopy, J Geophys Res-Atmos, 106, 7399-7414, Doi 10.1029/2000jd900679, 2001.

Brune, W. H., Baier, B. C., Thomas, J., Ren, X., Cohen, R. C., Pusede, S. E., Browne, E. C., Goldstein, A. H., Gentner, D. R., Keutsch, F. N., Thornton, J. A., Harrold, S., Lopez-Hilfiker, F. D., and Wennberg, P. O.: Ozone production chemistry in the
835   presence of urban plumes, Faraday Discuss, 189, 169-189, 10.1039/c5fd00204d, 2016.

Brune, W. H., Miller, D. O., Thames, A. B., Allen, H. M., Apel, E. C., Blake, D. R., Bui, T. P., Commane, R., Crounse, J. D., Daube, B. C., Diskin, G. S., DiGangi, J. P., Elkins, J. W., Hall, S. R., Hanisco, T. F., Hannun, R. A., Hintsa, E. J., Hornbrook, R. S., Kim, M. J., McKain, K., Moore, F. L., Neuman, J. A., Nicely, J. M., Peischl, J., Ryerson, T. B., St. Clair, J. M., Sweeney, C., Teng, A. P., Thompson, C., Ullmann, K., Veres, P. R., Wennberg, P. O., and Wolfe, G. M.: Exploring Oxidation in the
840   Remote Free Troposphere: Insights From Atmospheric Tomography (ATom), 125, e2019JD031685, https://doi.org/10.1029/2019JD031685, 2020.

Cárdenas, L. M., Austin, J. F., Burgess, R. A., Clemitshaw, K. C., Dorling, S., Penkett, S. A., and Harrison, R. M.: Correlations between CO, NO_y, O_3 and non-methane hydrocarbons and their relationships with meteorology during winter 1993 on the North Norfolk Coast, U.K, Atmospheric Environment, 32, 3339-3351, 10.1016/s1352-2310(97)00445-7, 1998.

Carpenter, L. J., Liss, P. S., and Penkett, S. A.: Marine organohalogens in the atmosphere over the Atlantic and Southern Oceans, J Geophys Res-Atmos, 108, 4256, Artn 4256
10.1029/2002jd002769, 2003.

Carpenter, L. J., Sturges, W. T., Penkett, S. A., Liss, P. S., Alicke, B., Hebestreit, K., and Platt, U.: Short-lived alkyl iodides and bromides at Mace Head, Ireland: Links to biogenic sources and halogen oxide production, J Geophys Res-Atmos, 104, 1679-1689, Doi 10.1029/98jd02746, 1999.

Chen, B. T., Cheng, Y. S., and Yeh, H. C.: Performance of a Tsi Aerodynamic Particle Sizer, Aerosol Sci Tech, 4, 89-97, Doi 10.1080/02786828508959041, 1985.

Commane, R., Seitz, K., Bale, C. S. E., Bloss, W. J., Buxmann, J., Platt, U., Pohler, D., Heard, D. E.: Iodine monoxide at a clean marine coastal site: observations of high frequency variations and inhomogeneous distributions, Atmos. Chem. Phys., 11, 6721-6733, 10.5194/acp-11-6721-2011, 2011.

Creasey, D. J., Evans, G. E., Heard, D. E., and Lee, J. D.: Measurements of OH and HO_2 concentrations in the Southern Ocean marine boundary layer, J Geophys Res-Atmos, 108, 4475, Artn 4475
10.1029/2002jd003206, 2003.

Creasey, D. J., HalfordMaw, P. A., Heard, D. E., Pilling, M. J., and Whitaker, B. J.: Implementation and initial deployment of a field instrument for measurement of OH and HO_2 in the troposphere by laser-induced fluorescence, J Chem Soc Faraday T, 93, 2907-2913, DOI 10.1039/a701469d, 1997.

Crilley, L. R., Kramer, L. J., Pope, F. D., Reed, C., Lee, J. D., Carpenter, L. J., Hollis, L. D. J., Ball, S. M., and Bloss, W. J.: Is the ocean surface a source of nitrous acid (HONO) in the marine boundary layer?, Atmos. Chem. Phys., 21, 18213-18225, 10.5194/acp-21-18213-2021, 2021.

Crounse, J. D., Nielsen, L. B., Jorgensen, S., Kjaergaard, H. G., and Wennberg, P. O.: Autoxidation of Organic Compounds in the Atmosphere, J Phys Chem Lett, 4, 3513-3520, 10.1021/jz4019207, 2013.

Crounse, J. D., Paulot, F., Kjaergaard, H. G., and Wennberg, P. O.: Peroxy radical isomerization in the oxidation of isoprene, Phys Chem Chem Phys, 13, 13607-13613, 10.1039/c1cp21330j, 2011.

Cryer, D. R.: Measurements of hydroxyl radical reactivity and formaldehyde in the atmosphere, PhD thesis, School of Chemistry, University of Leeds, 2016.

Di Carlo, P., Brune, W. H., Martinez, M., Harder, H., Lesher, R., Ren, X., Thornberry, T., Carroll, M. A., Young, V., Shepson, P. B., Riemer, D., Apel, E., and Campbell, C.: Missing OH reactivity in a forest: evidence for unknown reactive biogenic VOCs, Science, 304, 722-725, 10.1126/science.1094392, 2004.

27

Edwards, G. D., Cantrell, C. A., Stephens, S., Hill, B., Goyea, O., Shetter, R. E., Mauldin, R. L., 3rd, Kosciuch, E., Tanner, D.
875 J., and Eisele, F. L.: Chemical ionization mass spectrometer instrument for the measurement of tropospheric HO_2 and RO_2, Anal Chem, 75, 5317-5327, 10.1021/ac034402b, 2003.

Edwards, P. M., Evans, M. J., Furneaux, K. L., Hopkins, J., Ingham, T., Jones, C., Lee, J. D., Lewis, A. C., Moller, S. J., Stone, D., Whalley, L. K., and Heard, D. E.: OH reactivity in a South East Asian tropical rainforest during the Oxidant and Particle Photochemical Processes (OP3) project, Atmos Chem Phys, 13, 9497-9514, 10.5194/acp-13-9497-2013, 2013.

880 Ehhalt, D. H.: Photooxidation of trace gases in the troposphere Plenary Lecture, Physical Chemistry Chemical Physics, 1, 5401-5408, 10.1039/a905097c, 1999.

Ehn, M., Thornton, J. A., Kleist, E., Sipila, M., Junninen, H., Pullinen, I., Springer, M., Rubach, F., Tillmann, R., Lee, B., Lopez-Hilfiker, F., Andres, S., Acir, I. H., Rissanen, M., Jokinen, T., Schobesberger, S., Kangasluoma, J., Kontkanen, J., Nieminen, T., Kurten, T., Nielsen, L. B., Jorgensen, S., Kjaergaard, H. G., Canagaratna, M., Maso, M. D., Berndt, T., Petaja,
885 T., Wahner, A., Kerminen, V. M., Kulmala, M., Worsnop, D. R., Wildt, J., and Mentel, T. F.: A large source of low-volatility secondary organic aerosol, Nature, 506, 476-479, 10.1038/nature13032, 2014.

Emmerson, K. M., Carslaw, N., Carslaw, D. C., Lee, J. D., McFiggans, G., Bloss, W. J., Gravestock, T., Heard, D. E., Hopkins, J., Ingham, T., Pilling, M. J., Smith, S. C., Jacob, M., and Monks, P. S.: Free radical modelling studies during the UK TORCH Campaign in Summer 2003, Atmos Chem Phys, 7, 167-181, DOI 10.5194/acp-7-167-2007, 2007.

890 Faloona, I. C., Tan, D., Lesher, R. L., Hazen, N. L., Frame, C. L., Simpas, J. B., Harder, H., Martinez, M., Di Carlo, P., Ren, X. R., and Brune, W. H.: A laser-induced fluorescence instrument for detecting tropospheric OH and HO_2: Characteristics and calibration, Journal of Atmospheric Chemistry, 47, 139-167, DOI 10.1023/B:JOCH.0000021036.53185.0e, 2004.

Fleming, Z. L., Monks, P. S., Rickard, A. R., Bandy, B. J., Brough, N., Green, T. J., Reeves, C. E., and Penkett, S. A.: Seasonal dependence of peroxy radical concentrations at a Northern hemisphere marine boundary layer site during summer and winter:
895 evidence for radical activity in winter, Atmos. Chem. Phys., 6, 5415-5433, 10.5194/acp-6-5415-2006, 2006.

Forberich, O., Pfeiffer, T., Spiekermann, M., Walter, J., Comes, F. J., Grigonis, R., Clemitshaw, K. C., and Burgess, R. A.: Measurement of the Diurnal Variation of the OH Radical Concentration and Analysis of the Data by Modelling, Journal of Atmospheric Chemistry, 33, 155-181, 10.1023/A:1005973130335, 1999.

Fuchs, H., Bohn, B., Hofzumahaus, A., Holland, F., Lu, K. D., Nehr, S., Rohrer, F., and Wahner, A.: Detection of HO_2 by
900 laser-induced fluorescence: calibration and interferences from RO_2 radicals, Atmos Meas Tech, 4, 1209-1225, 10.5194/amt-4-1209-2011, 2011.

Fuchs, H., Holland, F., and Hofzumahaus, A.: Measurement of tropospheric RO_2 and HO_2 radicals by a laser-induced fluorescence instrument, Rev Sci Instrum, 79, 084104, 10.1063/1.2968712, 2008.

Fuchs, H., Tan, Z. F., Hofzumahaus, A., Broch, S., Dorn, H. P., Holland, F., Kunstler, C., Gomm, S., Rohrer, F., Schrade, S.,
905 Tillmann, R., and Wahner, A.: Investigation of potential interferences in the detection of atmospheric RO_x radicals by laser-induced fluorescence under dark conditions, Atmos Meas Tech, 9, 1431-1447, 10.5194/amt-9-1431-2016, 2016.

Furneaux, K. L.: Field Studies of the Chemistry of Free-Radicals in the Troposphere using Laser Induced Fluorescence Spectroscopy, PhD thesis, Ph.D., School of Chemistry, University of Leeds, Leeds, UK, 2009.

910 Green, T. J., Reeves, C. E., Fleming, Z. L., Brough, N., Rickard, A. R., Bandy, B. J., Monks, P. S., and Penkett, S. A.: An improved dual channel PERCA instrument for atmospheric measurements of peroxy radicals, Journal of environmental monitoring : JEM, 8, 530-536, 10.1039/b514630e, 2006.

Grenfell, J. L., Savage, N. H., Harrison, R. M., Penkett, S. A., Forberich, O., Comes, F. J., Clemitshaw, K. C., Burgess, R. A., Cárdenas, L. M., Davison, B., and McFadyen, G. G.: Tropospheric Box-Modelling and Analytical Studies of the Hydroxyl (OH) Radical and Related Species: Comparison with Observations, Journal of Atmospheric Chemistry, 33, 183-214,
915 10.1023/A:1006009901180, 1999.

Griffith, S. M., Hansen, R. F., Dusanter, S., Stevens, P. S., Alaghmand, M., Bertman, S. B., Carroll, M. A., Erickson, M., Galloway, M., Grossberg, N., Hottle, J., Hou, J., Jobson, B. T., Kammrath, A., Keutsch, F. N., Lefer, B. L., Mielke, L. H., O'Brien, A., Shepson, P. B., Thurlow, M., Wallace, W., Zhang, N., and Zhou, X. L.: OH and HO2 radical chemistry during PROPHET 2008 and CABINEX 2009-Part 1: Measurements and model comparison, Atmos Chem Phys, 13, 5403-5423,
920 10.5194/acp-13-5403-2013, 2013.

Guenther, A. B., Zimmerman, P. R., Harley, P. C., Monson, R. K., and Fall, R.: Isoprene and Monoterpene Emission Rate Variability - Model Evaluations and Sensitivity Analyses, J Geophys Res-Atmos, 98, 12609-12617, Doi 10.1029/93jd00527, 1993.

Hard, T. M., Obrien, R. J., Chan, C. Y., and Mehrabzadeh, A. A.: Tropospheric Free-Radical Determination by Fage, Environ
925 Sci Technol, 18, 768-777, DOI 10.1021/es00128a009, 1984.

Heard, D. E. and Pilling, M. J.: Measurement of OH and HO$_2$ in the troposphere, Chem Rev, 103, 5163-5198, 10.1021/cr020522s, 2003.

Heard, D. E., Read, K. A., Methven, J., Al-Haider, S., Bloss, W. J., Johnson, G. P., Pilling, M. J., Seakins, P. W., Smith, S. C., Sommariva, R., Stanton, J. C., Still, T. J., Ingham, T., Brooks, B., De Leeuw, G., Jackson, A. V., McQuaid, J. B., Morgan, R.,
930 Smith, M. H., Carpenter, L. J., Carslaw, N., Hamilton, J., Hopkins, J. R., Lee, J. D., Lewis, A. C., Purvis, R. M., Wevill, D. J., Brough, N., Green, T., Mills, G., Penkett, S. A., Plane, J. M. C., Saiz-Lopez, A., Worton, D., Monks, P. S., Fleming, Z., Rickard, A. R., Alfarra, M. R., Allan, J. D., Bower, K., Coe, H., Cubison, M., Flynn, M., McFiggans, G., Gallagher, M., Norton, E. G., O'Dowd, C. D., Shillito, J., Topping, D., Vaughan, G., Williams, P., Bitter, M., Ball, S. M., Jones, R. L., Povey, I. M., O'Doherty, S., Simmonds, P. G., Allen, A., Kinnersley, R. P., Beddows, D. C. S., Dall'Osto, M., Harrison, R. M.,
935 Donovan, R. J., Heal, M. R., Jennings, S. G., Noone, C., and Spain, G.: The North Atlantic Marine Boundary Layer Experiment (NAMBLEX). Overview of the campaign held at Mace Head, Ireland, in summer 2002, Atmos Chem Phys, 6, 2241-2272, DOI 10.5194/acp-6-2241-2006, 2006.

Heland, J., Kleefmann, J., Kurtenbach, R., and Wiesen, P.: A new instrument to measure gaseous nitrous acid (HONO) in the atmosphere, Environ Sci Technol, 35, 3207-3212, 10.1021/es000303t, 2001.

940 Hottle, J. R., Huisman, A. J., DiGangi, J. P., Kammrath, A., Galloway, M. M., Coens, K. L., and Keutsch, F. N.: A laser induced fluorescence-based instrument for in-situ measurements of atmospheric formaldehyde, Environ Sci Technol, 43, 790-795, 10.1021/es801621f, 2009.

Ingham, T., Goddard, A., Whalley, L. K., Furneaux, K. L., Edwards, P. M., Seal, C. P., Self, D. E., Johnson, G. P., Read, K. A., Lee, J. D., and Heard, D. E.: A flow-tube based laser-induced fluorescence instrument to measure OH reactivity in the troposphere, Atmos. Meas. Tech., 2, 465-477, 10.5194/amt-2-465-2009, 2009.

IPCC: Climate Change 2014 Synthesis Report, 2014.

Jeanneret, F., Kirchner, F., Clappier, A., van den Bergh, H., and Calpini, B.: Total VOC reactivity in the planetary boundary layer 1. Estimation by a pump and probe OH experiment, J Geophys Res-Atmos, 106, 3083-3093, Doi 10.1029/2000jd900602, 2001.

Jenkin, M. E., Saunders, S. M., Wagner, V., and Pilling, M. J.: Protocol for the development of the Master Chemical Mechanism, MCM v3 (Part B): tropospheric degradation of aromatic volatile organic compounds, Atmos Chem Phys, 3, 181-193, DOI 10.5194/acp-3-181-2003, 2003.

Jenkin, M. E., Young, J. C., and Rickard, A. R.: The MCM v3.3.1 degradation scheme for isoprene, Atmos Chem Phys, 15, 11433-11459, 10.5194/acp-15-11433-2015, 2015.

Jerrett, M., Burnett, R. T., Pope, C. A., 3rd, Ito, K., Thurston, G., Krewski, D., Shi, Y., Calle, E., and Thun, M.: Long-term ozone exposure and mortality, N Engl J Med, 360, 1085-1095, 10.1056/NEJMoa0803894, 2009.

Jokinen, T., Sipila, M., Richters, S., Kerminen, V. M., Paasonen, P., Stratmann, F., Worsnop, D., Kulmala, M., Ehn, M., Herrmann, H., and Berndt, T.: Rapid autoxidation forms highly oxidized RO2 radicals in the atmosphere, Angew Chem Int Ed Engl, 53, 14596-14600, 10.1002/anie.201408566, 2014.

Kanaya, Y. G., Cao, R. Q., Kato, S. G., Miyakawa, Y. K., Kajii, Y., Tanimoto, H., Yokouchi, Y., Mochida, M., Kawamura, K., and Akimoto, H.: Chemistry of OH and HO_2 radicals observed at Rishiri Island, Japan, in September 2003: Missing daytime sink of HO_2 and positive nighttime correlations with monoterpenes, J Geophys Res-Atmos, 112, D11308, Artn D11308 10.1029/2006jd007987, 2007.

Kebabian, P. L., Wood, E. C., Herndon, S. C., and Freedman, A.: A practical alternative to chemiluminescence-based detection of nitrogen dioxide: cavity attenuated phase shift spectroscopy, Environ Sci Technol, 42, 6040-6045, 10.1021/es703204j, 2008.

Keene, W. C., Long, M. S., Pszenny, A. A. P., Sander, R., Maben, J. R., Wall, A. J., O'Halloran, T. L., Kerkweg, A., Fischer, E. V., and Schrems, O.: Latitudinal variation in the multiphase chemical processing of inorganic halogens and related species over the eastern North and South Atlantic Oceans, Atmos Chem Phys, 9, 7361-7385, DOI 10.5194/acp-9-7361-2009, 2009.

Kovacs, T. A., Brune, W. H., Harder, H., Martinez, M., Simpas, J. B., Frost, G. J., Williams, E., Jobson, T., Stroud, C., Young, V., Fried, A., and Wert, B.: Direct measurements of urban OH reactivity during Nashville SOS in summer 1999, Journal of environmental monitoring : JEM, 5, 68-74, 10.1039/b204339d, 2003.

Krupa, S. V., Nosal, M., and Legge, A. H.: A numerical analysis of the combined open-top chamber data from the USA and Europe on ambient ozone and negative crop responses, Environ Pollut, 101, 157-160, https://doi.org/10.1016/S0269-7491(98)00019-0, 1998.

975   Kumar, V., Chandra, B. P., and Sinha, V.: Large unexplained suite of chemically reactive compounds present in ambient air due to biomass fires, Sci Rep, 8, 626, 10.1038/s41598-017-19139-3, 2018.

Lee, J. D., Moller, S. J., Read, K. A., Lewis, A. C., Mendes, L., and Carpenter, L. J.: Year-round measurements of nitrogen oxides and ozone in the tropical North Atlantic marine boundary layer, J Geophys Res-Atmos, 114, Artn D21302 10.1029/2009jd011878, 2009a.

980   Lee, J. D., Young, J. C., Read, K. A., Hamilton, J. F., Hopkins, J. R., Lewis, A. C., Bandy, B. J., Davey, J., Edwards, P., Ingham, T., Self, D. E., Smith, S. C., Pilling, M. J., and Heard, D. E.: Measurement and calculation of OH reactivity at a United Kingdom coastal site, J Atmos Chem, 64, 53-76, 10.1007/s10874-010-9171-0, 2009b.

Lewis, A., Carslaw, D., and Moller, S.: Non-methane Volatile Organic Compounds in the UK, 2020.

Lou, S., Holland, F., Rohrer, F., Lu, K., Bohn, B., Brauers, T., Chang, C. C., Fuchs, H., Haseler, R., Kita, K., Kondo, Y., Li, 985   X., Shao, M., Zeng, L., Wahner, A., Zhang, Y., Wang, W., and Hofzumahaus, A.: Atmospheric OH reactivities in the Pearl River Delta - China in summer 2006: measurement and model results, Atmos Chem Phys, 10, 11243-11260, 10.5194/acp-10-11243-2010, 2010.

Lu, K. D., Hofzumahaus, A., Holland, F., Bohn, B., Brauers, T., Fuchs, H., Hu, M., Häseler, R., Kita, K., Kondo, Y., Li, X., Lou, S. R., Oebel, A., Shao, M., Zeng, L. M., Wahner, A., Zhu, T., Zhang, Y. H., and Rohrer, F.: Missing OH source in a 990   suburban environment near Beijing: observed and modelled OH and HO_2 concentrations in summer 2006, Atmos Chem Phys, 13, 1057-1080, 10.5194/acp-13-1057-2013, 2013.

Lu, K. D., Rohrer, F., Holland, F., Fuchs, H., Bohn, B., Brauers, T., Chang, C. C., Haseler, R., Hu, M., Kita, K., Kondo, Y., Li, X., Lou, S. R., Nehr, S., Shao, M., Zeng, L. M., Wahner, A., Zhang, Y. H., and Hofzumahaus, A.: Observation and modelling of OH and HO_2 concentrations in the Pearl River Delta 2006: a missing OH source in a VOC rich atmosphere, 995   Atmos Chem Phys, 12, 1541-1569, 10.5194/acp-12-1541-2012, 2012.

Madronich, S.: Implications of recent total atmospheric ozone measurements for biologically active ultraviolet radiation reaching the Earth's surface, Geophys Res Lett, 19, 37-40, 10.1029/91gl02954, 1992.

Mallik, C., Tomsche, L., Bourtsoukidis, E., Crowley, J. N., Derstroff, B., Fischer, H., Hafermann, S., Huser, I., Javed, U., Kessel, S., Lelieveld, J., Martinez, M., Meusel, H., Novelli, A., Phillips, G. J., Pozzer, A., Reiffs, A., Sander, R., Taraborrelli, 1000 D., Sauvage, C., Schuladen, J., Su, H., Williams, J., and Harder, H.: Oxidation processes in the eastern Mediterranean atmosphere: evidence from the modelling of HOx measurements over Cyprus, Atmos Chem Phys, 18, 10825-10847, 10.5194/acp-18-10825-2018, 2018.

Mao, J., Ren, X., Brune, W. H., Olson, J. R., Crawford, J. H., Fried, A., Huey, L. G., Cohen, R. C., Heikes, B., Singh, H. B., Blake, D. R., Sachse, G. W., Diskin, G. S., Hall, S. R., and Shetter, R. E.: Airborne measurement of OH reactivity during 1005 INTEX-B, Atmos Chem Phys, 9, 163-173, 10.5194/acp-9-163-2009, 2009.

Mao, J., Ren, X., Zhang, L., Van Duin, D. M., Cohen, R. C., Park, J. H., Goldstein, A. H., Paulot, F., Beaver, M. R., Crounse, J. D., Wennberg, P. O., DiGangi, J. P., Henry, S. B., Keutsch, F. N., Park, C., Schade, G. W., Wolfe, G. M., Thornton, J. A., and Brune, W. H.: Insights into hydroxyl measurements and atmospheric oxidation in a California forest, Atmos Chem Phys, 12, 8009-8020, 10.5194/acp-12-8009-2012, 2012.

1010 McFiggans, G., Coe, H., Burgess, R., Allan, J., Cubison, M., Alfarra, M. R., Saunders, R., Saiz-Lopez, A., Plane, J. M. C., Wevill, D., Carpenter, L., Rickard, A. R., and Monks, P. S.: Direct evidence for coastal iodine particles from Laminaria macroalgae – linkage to emissions of molecular iodine, Atmos Chem Phys, 4, 701-713, 10.5194/acp-4-701-2004, 2004.

Mehra, A., Wang, Y., Krechmer, J. E., Lambe, A., Majluf, F., Morris, M. A., Priestley, M., Bannan, T. J., Bryant, D. J., Pereira, K. L., Hamilton, J. F., Rickard, A. R., Newland, M. J., Stark, H., Croteau, P., Jayne, J. T., Worsnop, D. R., Canagaratna, M.
1015 R., Wang, L., and Coe, H.: Evaluation of the Chemical Composition of Gas and Particle Phase Products of Aromatic Oxidation, Atmos. Chem. Phys. Discuss., 2020, 1-24, 10.5194/acp-2020-161, 2020.

Molteni, U., Bianchi, F., Klein, F., El Haddad, I., Frege, C., Rossi, M. J., Dommen, J., and Baltensperger, U.: Formation of highly oxygenated organic molecules from aromatic compounds, Atmos Chem Phys, 18, 1909-1921, 10.5194/acp-18-1909-2018, 2018.

1020 Murphy, J. G., Oram, D. E., and Reeves, C. E.: Measurements of volatile organic compounds over West Africa, Atmos Chem Phys, 10, 5281-5294, 10.5194/acp-10-5281-2010, 2010.

Nash, T.: The colorimetric estimation of formaldehyde by means of the Hantzsch reaction, Biochem J, 55, 416-421, 1953.

Nolscher, A. C., Williams, J., Sinha, V., Custer, T., Song, W., Johnson, A. M., Axinte, R., Bozem, H., Fischer, H., Pouvesle, N., Phillips, G., Crowley, J. N., Rantala, P., Rinne, J., Kulmala, M., Gonzales, D., Valverde-Canossa, J., Vogel, A., Hoffmann, T., Ouwersloot, H. G., de Arellano, J. V. G., and Lelieveld, J.: Summertime total OH reactivity measurements from boreal forest during HUMPPA-COPEC 2010, Atmos Chem Phys, 12, 8257-8270, 10.5194/acp-12-8257-2012, 2012.

Novelli, A., Hens, K., Ernest, C. T., Kubistin, D., Regelin, E., Elste, T., Plass-Dulmer, C., Martinez, M., Lelieveld, J., and Harder, H.: Characterisation of an inlet pre-injector laser-induced fluorescence instrument for the measurement of atmospheric hydroxyl radicals, Atmos Meas Tech, 7, 3413-3430, 10.5194/amt-7-3413-2014, 2014a.

1030 Novelli, A., Vereecken, L., Lelieveld, J., and Harder, H.: Direct observation of OH formation from stabilised Criegee intermediates, Phys Chem Chem Phys, 16, 19941-19951, 10.1039/c4cp02719a, 2014b.

Orlando, J. J. and Tyndall, G. S.: Laboratory studies of organic peroxy radical chemistry: an overview with emphasis on recent issues of atmospheric significance, Chem Soc Rev, 41, 6294-6317, 10.1039/c2cs35166h, 2012.

Penkett, S. A., Clemitshaw, K. C., Savage, N. H., Burgess, R. A., Cardenas, L. M., Carpenter, L. J., McFadyen, G. G., and
1035 Cape, J. N.: Studies of oxidant production at the Weybourne Atmospheric Observatory in summer and winter conditions, Journal of Atmospheric Chemistry, 33, 111-128, Doi 10.1023/A:1005969204215, 1999.

Ravishankara, A. R.: Heterogeneous and multiphase chemistry in the troposphere, Science, 276, 1058-1065, DOI 10.1126/science.276.5315.1058, 1997.

Reed, C., Brumby, C. A., Crilley, L. R., Kramer, L. J., Bloss, W. J., Seakins, P. W., Lee, J. D., and Carpenter, L. J.: HONO
1040 measurement by differential photolysis, Atmos Meas Tech, 9, 2483-2495, 10.5194/amt-9-2483-2016, 2016.

Ren, X. R., Harder, H., Martinez, M., Lesher, R. L., Oliger, A., Shirley, T., Adams, J., Simpas, J. B., and Brune, W. H.: HO_x concentrations and OH reactivity observations in New York City during PMTACS-NY2001, Atmospheric Environment, 37, 3627-3637, 10.1016/S1352-2310(03)00460-6, 2003.

1045   Ren, X. R., Olson, J. R., Crawford, J. H., Brune, W. H., Mao, J. Q., Long, R. B., Chen, Z., Chen, G., Avery, M. A., Sachse, G. W., Barrick, J. D., Diskin, G. S., Huey, L. G., Fried, A., Cohen, R. C., Heikes, B., Wennberg, P. O., Singh, H. B., Blake, D. R., and Shetter, R. E.: HO_x chemistry during INTEX-A 2004: Observation, model calculation, and comparison with previous studies, J Geophys Res-Atmos, 113, D05310, Artn D05310
10.1029/2007jd009166, 2008.

Robbins, R. C., Borg, K. M., and Robinson, E.: Carbon monoxide in the atmosphere, J Air Pollut Control Assoc, 18, 106-110,
1050   10.1080/00022470.1968.10469094, 1968.

Rohrer, F. and Berresheim, H.: Strong correlation between levels of tropospheric hydroxyl radicals and solar ultraviolet radiation, Nature, 442, 184-187, 10.1038/nature04924, 2006.

Sadanaga, Y., Yoshino, A., Watanabe, K., Yoshioka, A., Wakazono, Y., Kanaya, Y., and Kajii, Y.: Development of a measurement system of OH reactivity in the atmosphere by using a laser-induced pump and probe technique, Review of
1055   Scientific Instruments, 75, 2648-2655, 10.1063/1.1775311, 2004.

Salisbury, G., Rickard, A. R., Monks, P. S., Allan, B. J., Bauguitte, S., Penkett, S. A., Carslaw, N., Lewis, A. C., Creasey, D. J., Heard, D. E., Jacobs, P. J., and Lee, J. D.: Production of peroxy radicals at night via reactions of ozone and the nitrate radical in the marine boundary layer, Journal of Geophysical Research: Atmospheres, 106, 12669-12687, 10.1029/2000jd900754, 2001.

1060   Saunders, S. M., Jenkin, M. E., Derwent, R. G., and Pilling, M. J.: World Wide Web site of a Master Chemical Mechanism (MCM) for use in tropospheric chemistry models, Atmospheric Environment, 31, 1249-1249, Doi 10.1016/S1352-2310(97)85197-7, 1997.

Saunders, S. M., Jenkin, M. E., Derwent, R. G., and Pilling, M. J.: Protocol for the development of the Master Chemical Mechanism, MCM v3 (Part A): tropospheric degradation of non-aromatic volatile organic compounds, Atmos Chem Phys, 3,
1065   161-180, DOI 10.5194/acp-3-161-2003, 2003.

Sinha, V., Williams, J., Crowley, J. N., and Lelieveld, J.: The comparative reactivity method - a new tool to measure total OH reactivity in ambient air, Atmos Chem Phys, 8, 2213-2227, DOI 10.5194/acp-8-2213-2008, 2008.

Sinha, V., Williams, J., Diesch, J. M., Drewnick, F., Martinez, M., Harder, H., Regelin, E., Kubistin, D., Bozem, H., Hosaynali-Beygi, Z., Fischer, H., Andres-Hernandez, M. D., Kartal, D., Adame, J. A., and Lelieveld, J.: Constraints on instantaneous
1070   ozone production rates and regimes during DOMINO derived using in-situ OH reactivity measurements, Atmos Chem Phys, 12, 7269-7283, 10.5194/acp-12-7269-2012, 2012.

Slater, E. J., Whalley, L. K., Woodward-Massey, R., Ye, C., Lee, J. D., Squires, F., Hopkins, J. R., Dunmore, R. E., Shaw, M., Hamilton, J. F., Lewis, A. C., Crilley, L. R., Kramer, L., Bloss, W., Vu, T., Sun, Y., Xu, W., Yue, S., Ren, L., Acton, W. J. F., Hewitt, C. N., Wang, X., Fu, P., and Heard, D. E.: Elevated levels of OH observed in haze events during wintertime in central
1075   Beijing, Atmos. Chem. Phys. Discuss., 2020, 1-43, 10.5194/acp-2020-362, 2020.

Atmospheric
Chemistry
and Physics

Discussions

Smith, S. C.: Atmospheric measurements of OH and HO_2 using the FAGE technique: Instrument development and data analysis, PhD thesis, School of Chemistry, University of Leeds, 2007.

Smith, S. C., Lee, J. D., Bloss, W. J., Johnson, G. P., Ingham, T., and Heard, D. E.: Concentrations of OH and HO_2 radicals during NAMBLEX: measurements and steady state analysis, Atmos Chem Phys, 6, 1435-1453, DOI 10.5194/acp-6-1435-2006, 2006.

Sommariva, R., Bates, T. S., Bon, D., Brookes, D. M., de Gouw, J. A., Gilman, J. B., Herndon, S. C., Kuster, W. C., Lerner, B. M., Monks, P. S., Osthoff, H. D., Parker, A. E., Roberts, J. M., Tucker, S. C., Warneke, C., Williams, E. J., Zahniser, M. S., and Brown, S. S.: Modelled and measured concentrations of peroxy radicals and nitrate radical in the U.S. Gulf Coast region during TexAQS 2006, Journal of Atmospheric Chemistry, 68, 331-362, 10.1007/s10874-012-9224-7, 2011.

Sommariva, R., Bloss, W. J., Brough, N., Carslaw, N., Flynn, M., Haggerstone, A. L., Heard, D. E., Hopkins, J. R., Lee, J. D., Lewis, A. C., McFiggans, G., Monks, P. S., Penkett, S. A., Pilling, M. J., Plane, J. M. C., Read, K. A., Saiz-Lopez, A., Rickard, A. R., and Williams, P. I.: OH and HO_2 chemistry during NAMBLEX: roles of oxygenates, halogen oxides and heterogeneous uptake, Atmos Chem Phys, 6, 1135-1153, DOI 10.5194/acp-6-1135-2006, 2006.

Sommariva, R., Cox, S., Martin, C., Borońska, K., Young, J., Jimack, P. K., Pilling, M. J., Matthaios, V. N., Nelson, B. S., Newland, M. J., Panagi, M., Bloss, W. J., Monks, P. S., and Rickard, A. R.: AtChem (version 1), an open-source box model for the Master Chemical Mechanism, Geosci. Model Dev., 13, 169-183, 10.5194/gmd-13-169-2020, 2020.

Sommariva, R., Haggerstone, A. L., Carpenter, L. J., Carslaw, N., Creasey, D. J., Heard, D. E., Lee, J. D., Lewis, A. C., Pilling, M. J., and Zador, J.: OH and HO_2 chemistry in clean marine air during SOAPEX-2, Atmos Chem Phys, 4, 839-856, DOI 10.5194/acp-4-839-2004, 2004.

Sommariva, R., Hollis, L., Sherwen, T., R Baker, A., M Ball, S., J Bandy, B., G Bell, T., N Chowdhury, M., Cordell, R., Evans, M., D Lee, J., Reed, C., E Reeves, C., M Roberts, J., Yang, M., and Monks, P.: Seasonal and geographical variability of nitryl chloride and its precursors in Northern Europe, e844 pp., 10.1002/asl.844, 2018.

Song, H., Chen, X., Lu, K., Zou, Q., Tan, Z., Fuchs, H., Wiedensohler, A., Moon, D. R., Heard, D. E., Baeza-Romero, M. T., Zheng, M., Wahner, A., Kiendler-Scharr, A., and Zhang, Y.: Influence of aerosol copper on HO2 uptake: a novel parameterized equation, Atmos. Chem. Phys., 20, 15835-15850, 10.5194/acp-20-15835-2020, 2020.

Stone, D., Sherwen, T., Evans, M. J., Vaughan, S., Ingham, T., Whalley, L. K., Edwards, P. M., Read, K. A., Lee, J. D., Moller, S. J., Carpenter, L. J., Lewis, A. C., and Heard, D. E.: Impacts of bromine and iodine chemistry on tropospheric OH and HO_2: comparing observations with box and global model perspectives, Atmos Chem Phys, 18, 3541-3561, 10.5194/acp-18-3541-2018, 2018.

Stone, D., Whalley, L. K., and Heard, D. E.: Tropospheric OH and HO_2 radicals: field measurements and model comparisons, Chem Soc Rev, 41, 6348-6404, 10.1039/c2cs35140d, 2012.

Stone, D., Whalley, L. K., Ingham, T., Edwards, P. M., Cryer, D. R., Brumby, C. A., Seakins, P. W., and Heard, D. E.: Measurement of OH reactivity by laser flash photolysis coupled with laser-induced fluorescence spectroscopy, Atmos Meas Tech, 9, 2827-2844, 10.5194/amt-9-2827-2016, 2016.

1110 Tan, Z., Lu, K., Hofzumahaus, A., Fuchs, H., Bohn, B., Holland, F., Liu, Y., Rohrer, F., Shao, M., Sun, K., Wu, Y., Zeng, L., Zhang, Y., Zou, Q., Kiendler-Scharr, A., Wahner, A., and Zhang, Y.: Experimental budgets of OH, HO$_2$ and RO$_2$ radicals and implications for ozone formation in the Pearl River Delta in China 2014, Atmospheric Chemistry and Physics Discussions, 2018, 1-28, 10.5194/acp-2018-801, 2018a.

Tan, Z. F., Fuchs, H., Lu, K. D., Hofzumahaus, A., Bohn, B., Broch, S., Dong, H. B., Gomm, S., Haseler, R., He, L. Y.,
1115 Holland, F., Li, X., Liu, Y., Lu, S. H., Rohrer, F., Shao, M., Wang, B. L., Wang, M., Wu, Y. S., Zeng, L. M., Zhang, Y. S., Wahner, A., and Zhang, Y. H.: Radical chemistry at a rural site (Wangdu) in the North China Plain: observation and model calculations of OH, HO$_2$ and RO$_2$ radicals, Atmos Chem Phys, 17, 663-690, 10.5194/acp-17-663-2017, 2017.

Tan, Z. F., Rohrer, F., Lu, K. D., Ma, X. F., Bohn, B., Broch, S., Dong, H. B., Fuchs, H., Gkatzelis, G. I., Hofzumahaus, A., Holland, F., Li, X., Liu, Y., Liu, Y. H., Novelli, A., Shao, M., Wang, H. C., Wu, Y. S., Zeng, L. M., Hu, M., Kiendler-Scharr,
1120 A., Wahner, A., and Zhang, Y. H.: Wintertime photochemistry in Beijing: observations of RO$_x$ radical concentrations in the North China Plain during the BEST-ONE campaign, Atmos Chem Phys, 18, 12391-12411, 10.5194/acp-18-12391-2018, 2018b.

Thames, A. B., Brune, W. H., Miller, D. O., Allen, H. M., Apel, E. C., Blake, D. R., Bui, T. P., Commane, R., Crounse, J. D., Daube, B. C., Diskin, G. S., DiGangi, J. P., Elkins, J. W., Hall, S. R., Hanisco, T. F., Hannun, R. A., Hintsa, E., Hornbrook,
1125 R. S., Kim, M. J., McKain, K., Moore, F. L., Nicely, J. M., Peischl, J., Ryerson, T. B., St. Clair, J. M., Sweeney, C., Teng, A., Thompson, C. R., Ullmann, K., Wennberg, P. O., and Wolfe, G. M.: Missing OH reactivity in the global marine boundary layer, Atmos. Chem. Phys., 20, 4013-4029, 10.5194/acp-20-4013-2020, 2020.

van Stratum, B. J. H., Vilà-Guerau de Arellano, J., Ouwersloot, H. G., van den Dries, K., van Laar, T. W., Martinez, M., Lelieveld, J., Diesch, J. M., Drewnick, F., Fischer, H., Hosaynali Beygi, Z., Harder, H., Regelin, E., Sinha, V., Adame, J. A.,
1130 Sörgel, M., Sander, R., Bozem, H., Song, W., Williams, J., and Yassaa, N.: Case study of the diurnal variability of chemically active species with respect to boundary layer dynamics during DOMINO, Atmos Chem Phys, 12, 5329-5341, 10.5194/acp-12-5329-2012, 2012.

Vaughan, S., Ingham, T., Whalley, L. K., Stone, D., Evans, M. J., Read, K. A., Lee, J. D., Moller, S. J., Carpenter, L. J., Lewis, A. C., Fleming, Z. L., and Heard, D. E.: Seasonal observations of OH and HO$_2$ in the remote tropical marine boundary layer,
1135 Atmos Chem Phys, 12, 2149-2172, 10.5194/acp-12-2149-2012, 2012.

Wang, S., Wu, R., Berndt, T., Ehn, M., and Wang, L.: Formation of Highly Oxidized Radicals and Multifunctional Products from the Atmospheric Oxidation of Alkylbenzenes, Environ Sci Technol, 51, 8442-8449, 10.1021/acs.est.7b02374, 2017.

Wang, Y., Mehra, A., Krechmer, J. E., Yang, G., Hu, X., Lu, Y., Lambe, A., Canagaratna, M., Chen, J., Worsnop, D., Coe, H., and Wang, L.: Oxygenated products formed from OH-initiated reactions of trimethylbenzene: Autoxidation and accretion,
1140 Atmos. Chem. Phys. Discuss., 2020, 1-32, 10.5194/acp-2020-165, 2020.

Whalley, L. K., Blitz, M. A., Desservettaz, M., Seakins, P. W., and Heard, D. E.: Reporting the sensitivity of laser-induced fluorescence instruments used for HO$_2$ detection to an interference from RO$_2$ radicals and introducing a novel approach that enables HO$_2$ and certain RO$_2$ types to be selectively measured, Atmos Meas Tech, 6, 3425-3440, 10.5194/amt-6-3425-2013, 2013.

1145 Whalley, L. K., Furneaux, K. L., Goddard, A., Lee, J. D., Mahajan, A., Oetjen, H., Read, K. A., Kaaden, N., Carpenter, L. J., Lewis, A. C., Plane, J. M. C., Saltzman, E. S., Wiedensohler, A., and Heard, D. E.: The chemistry of OH and HO_2 radicals in the boundary layer over the tropical Atlantic Ocean, Atmos Chem Phys, 10, 1555-1576, 10.5194/acp-10-1555-2010, 2010.

Whalley, L. K., Slater, E. J., Woodward-Massey, R., Ye, C., Lee, J. D., Squires, F., Hopkins, J. R., Dunmore, R. E., Shaw, M., Hamilton, J. F., Lewis, A. C., Mehra, A., Worrall, S. D., Bacak, A., Bannan, T. J., Coe, H., Ouyang, B., Jones, R. L., Crilley,
1150 L. R., Kramer, L. J., Bloss, W. J., Vu, T., Kotthaus, S., Grimmond, S., Sun, Y., Xu, W., Yue, S., Ren, L., Acton, W. J. F., Hewitt, C. N., Wang, X., Fu, P., and Heard, D. E.: Evaluating the sensitivity of radical chemistry and ozone formation to ambient VOCs and NOx in Beijing, Atmos. Chem. Phys. Discuss., 2020, 1-41, 10.5194/acp-2020-785, 2020.

Whalley, L. K., Stone, D., Bandy, B., Dunmore, R., Hamilton, J. F., Hopkins, J., Lee, J. D., Lewis, A. C., and Heard, D. E.: Atmospheric OH reactivity in central London: observations, model predictions and estimates of in situ ozone production,
1155 Atmos. Chem. Phys., 16, 2109-2122, 10.5194/acp-16-2109-2016, 2016.

Whalley, L. K., Stone, D., Dunmore, R., Hamilton, J., Hopkins, J. R., Lee, J. D., Lewis, A. C., Williams, P., Kleffmann, J., Laufs, S., Woodward-Massey, R., and Heard, D. E.: Understanding in situ ozone production in the summertime through radical observations and modelling studies during the Clean air for London project (ClearfLo), Atmos Chem Phys, 18, 2547-2571, 10.5194/acp-18-2547-2018, 2018.

1160 Woodward-Massey, R.: Observations of radicals in the atmosphere: measurement validation and model comparisons, PhD Thesis, School of Chemistry, University of Leeds, 2018.

Woodward-Massey, R., Slater, E. J., Alen, J., Ingham, T., Cryer, D. R., Stimpson, L. M., Ye, C., Seakins, P. W., Whalley, L. K., and Heard, D. E.: Implementation of a chemical background method for atmospheric OH measurements by laser-induced fluorescence: characterisation and observations from the UK and China, Atmos. Meas. Tech., 13, 3119-3146, 10.5194/amt-
1165 13-3119-2020, 2020.

Woodward-Massey, R., Sommariva, R., Whalley, L. K., Cryer, D. R., Ingham, T., Bloss, W. J., Cox, S., Lee, J. D., Reed, C., Crilley, L. R., Kramer, L. J., Bandy, B. J., Forster, G. L., Reeves, C. E., Monks, P. S., and Heard, D. E.: Radical chemistry at a UK coastal receptor site – Part 2: experimental radical budgets and ozone production, Submitted, 2022.

Zannoni, N., Gros, V., Esteve, R. S., Kalogridis, C., Michoud, V., Dusanter, S., Sauvage, S., Locoge, N., Colomb, A., and
1170 Bonsang, B.: Summertime OH reactivity from a receptor coastal site in the Mediterranean Basin, Atmos Chem Phys, 17, 12645-12658, 10.5194/acp-17-12645-2017, 2017.

Zha, Q., Yan, C., Junninen, H., Riva, M., Aalto, J., Quéléver, L., Schallhart, S., Dada, L., Heikkinen, L., Peräkylä, O., Zou, J., Rose, C., Wang, Y., Mammarella, I., Katul, G., Vesala, T., Worsnop, D. R., Kulmala, M., Petäjä, T., Bianchi, F., and Ehn, M.: Vertical characterization of Highly Oxygenated Molecules (HOMs) below and above a boreal forest canopy, Atmospheric
1175 Chemistry and Physics Discussions, 2017, 1-32, 10.5194/acp-2017-1098, 2017.

Zhang, L., Brook, J. R., and Vet, R.: A revised parameterization for gaseous dry deposition in air-quality models, Atmos Chem Phys, 3, 2067-2082, DOI 10.5194/acp-3-2067-2003, 2003.

1180

1185

Tables

Atmospheric
Chemistry
and Physics
Discussions
Open Access
EGU

Table 1. List of species observed and their corresponding measurement techniques for the ICOZA campaign. For descriptions of simple and complex RO_2, see Section 2.1.2. For some species (e.g., NO, NO_2, HONO, HCHO) more than one measurement technique was available.

Observation(s)	Technique	Sampling platform	Institution	Reference(s)
OH, HO_2, total RO_2, "simple" and "complex" RO_2	Fluorescence assay by gas expansion (FAGE)	FAGE container roof	Leeds	Whalley et al. (2013); Whalley et al. (2018); Woodward-Massey et al. (2020)
OH reactivity	Laser flash photolysis–laser-induced fluorescence spectroscopy (LFP-LIF)	FAGE container roof	Leeds	Stone et al. (2016)
$J(O^1D)$	Filter radiometry	FAGE container roof	Leeds	Bohn et al. (2016)
Photolysis frequencies	Spectral radiometry (two instruments)	FAGE and Leicester containers	Leeds/Leicester	Bohn et al. (2008)
HCHO	Laser-induced fluorescence (LIF)	WAO manifold	Leeds	Cryer (2016)
HONO	Long path absorption photometry (LOPAP)	Birmingham van roof	Birmingham	Heland et al. (2001); Crilley et al. (2021)
Aerosol surface area	Aerodynamic particle sizer (APS)	Birmingham van roof	Birmingham	Chen et al. (1985)
$Cl_2/ClNO_2$	Chemical ionisation mass spectrometry	Leicester container roof	Leicester	Sommariva et al. (2018)
NO (NO_2)	Chemiluminescence (LED NO_2 converter)	WAO roof	York	Lee et al. (2009a)
NO_2	Cavity-attenuated phase-shift spectroscopy (CAPS)	WAO manifold	York	Kebabian et al. (2008)
HONO	Differential photolysis with chemiluminescence detection of NO	WAO roof	York	Reed et al. (2016)
O_3	UV absorption	WAO manifold	UEA	-
CO	MgO reduction with UV detection	WAO manifold	UEA	Robbins et al. (1968)
HCHO	Hantzsch colourimetry	WAO manifold	UEA	Nash (1953)
VOCs (up to C_6 alkanes/alkenes, acetylene, benzene, toluene)	Gas chromatography with flame ionisation detection (GC-FID)	WAO roof	UEA	-
VOCs (C_8/C_9 aromatics, Σmonoterpenes), OVOCs (methanol, acetaldehyde, acetone, acetic acid, MVK+MACR[a], MEK[b]), acetonitrile, DMS[c]	Proton transfer reaction–mass spectrometry (PTR-MS)	WAO roof	UEA	Murphy et al. (2010)

[a]Sum of methyl vinyl ketone and methacrolein.

[b]Methyl ethyl ketone.

5 [c]Dimethyl sulfide.

Table 2. Median trace gas mixing ratios and meteorological parameters, split according to wind direction (NW–SE = <165° and >285°; SW = 180°–270°).

Species or meteorological parameter	NW-SE air	SW air
NO (pptv)	142	233
NO$_2$ (pptv)	1854	2766
HONO (pptv)	52	97
CO (ppbv)	113	106
O$_3$ (ppbv)	39	31
HCHO (pptv)	925	1127
Isoprene (pptv)	27	34
MVK+MACR (pptv)	40	88
PM$_{2.5}$ (μg/m^3)	3.8	4.4
Temp (°C)	15.7	17.4
RH (%)	82	72
$J(O^1D)$ (s^{-1})[a]	1.7×10^{-5}	1.4×10^{-5}

[a]Reported as the maxima in Figure 4.

Atmospheric
Chemistry
and Physics
Discussions

Table 3. Fit parameters obtained from power law fits ($y = y0 + Ax^{\mathrm{pow}}$) to the OH vs $J(O^1D)$ data shown in Figure 9, split according to wind direction (NW–SE = <165° and >285°; SW = 180°–270°).

	NW-SE		*SW*	
	Observed	*MCM-base*	*Observed*	*MCM-base*
$y0$	1.2×10^5	1.4×10^4	1.8×10^5	1.0×10^5
A	7.2×10^{11}	3.7×10^9	1.1×10^{10}	5.2×10^{10}
pow	0.86	0.61	0.67	0.80

Table 4. Fit parameters obtained from linear fits (y = mx + c, with number of points, N, and Pearson correlation coefficient, R) to the RO_2 vs HO_2 data shown in Figure 10, split according to wind direction (NW–SE = <165° and >285°; SW = 180°–270°).

	NW-SE		*SW*	
	Observed	*MCM-base* [a]	*Observed*	*MCM-base* [a]
m	1.3	0.67	1.8	0.63
c	1.6×10^8	9.6×10^6	1.20×10^8	-3.50×10^6
N	373	113	451	122
R	0.63	0.96	0.81	0.97

[a]Nighttime data not included.

Figures
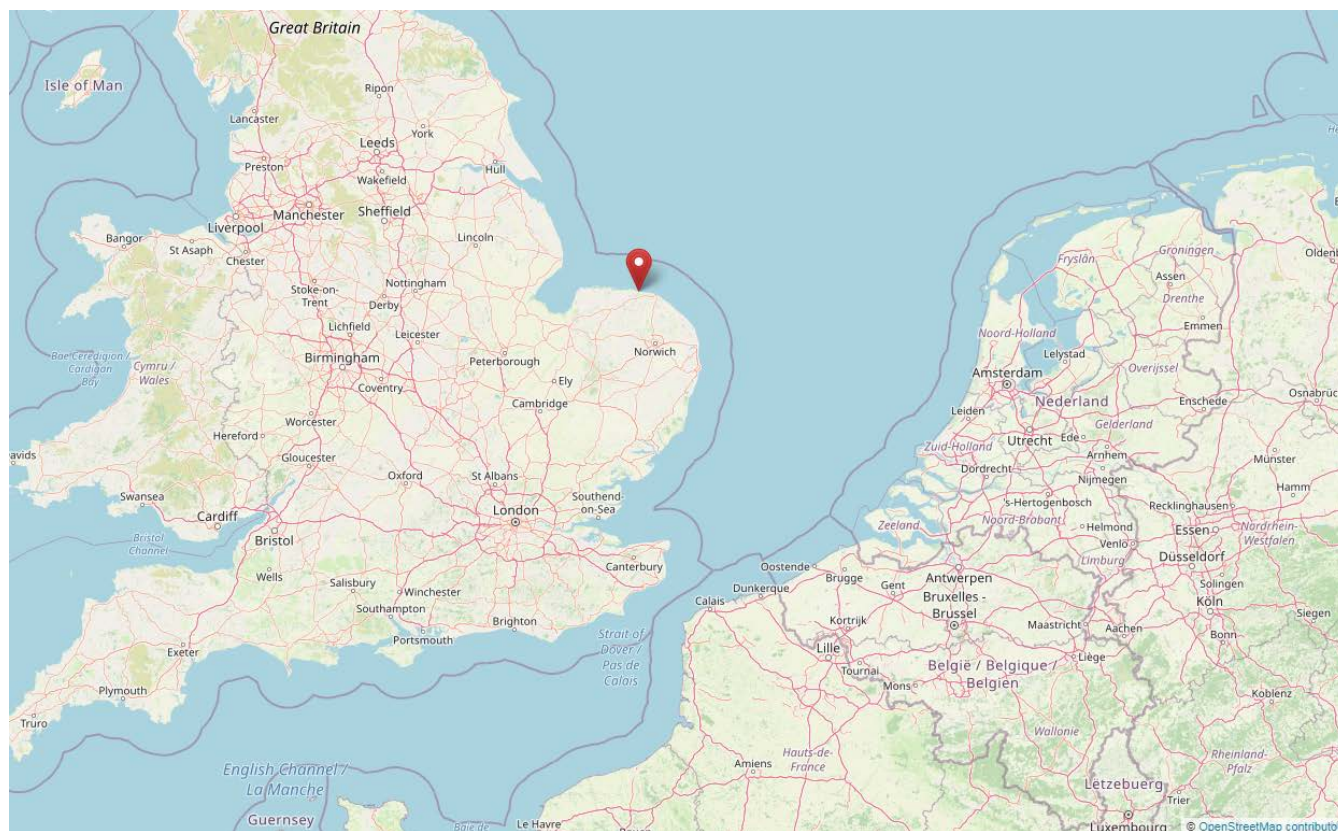
Figure 1. Location (red pin) of the Weybourne Atmospheric Observatory (WAO) on the North Norfolk coast (52°57'02" N, 1°07'19"E, 16 m above sea level). © OpenStreetMap contributors 2022. Distributed under the Open Data Commons Open Database License (ODbL) v1.0.

5
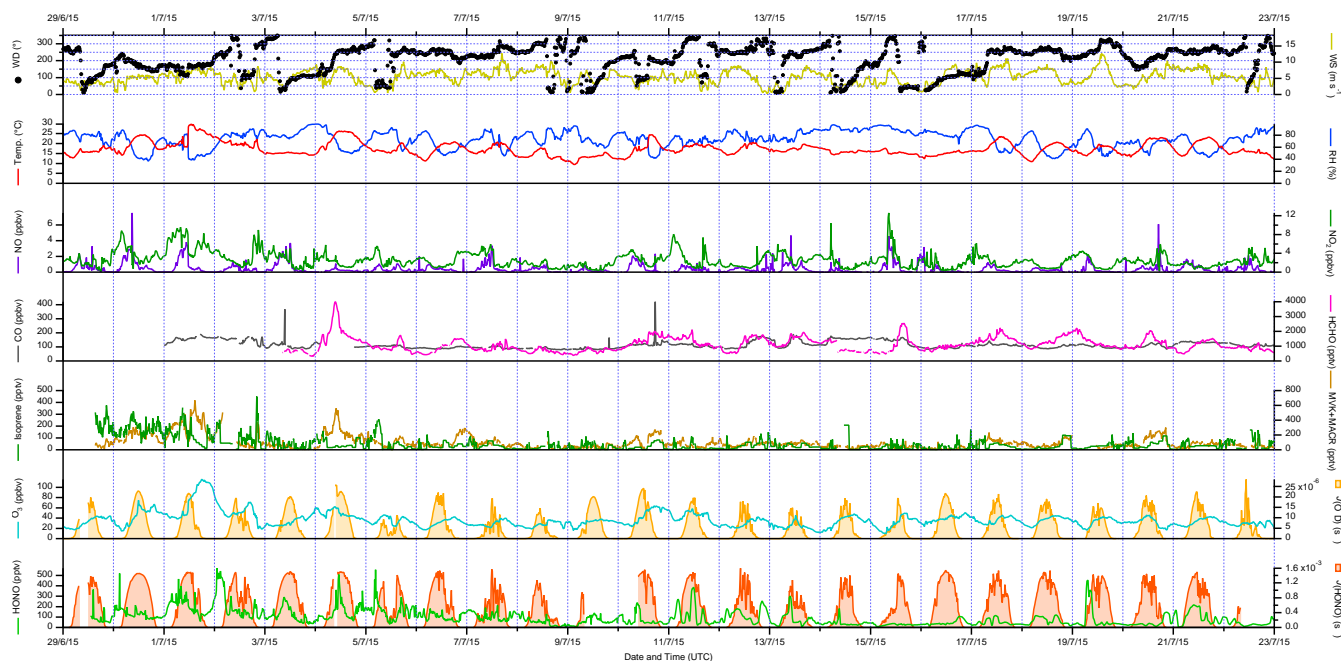
Figure 2. Time series of meteorological parameters (wind speed and direction, temperature, RH, photolysis frequencies) and trace gases (NO, NO₂, CO, HCHO, isoprene, MVK+MACR, O₃, HONO) measured during ICOZA (29th June – 23rd July 2015). All data presented are 15 min averages. UTC = Universal Time Coordinated.

5
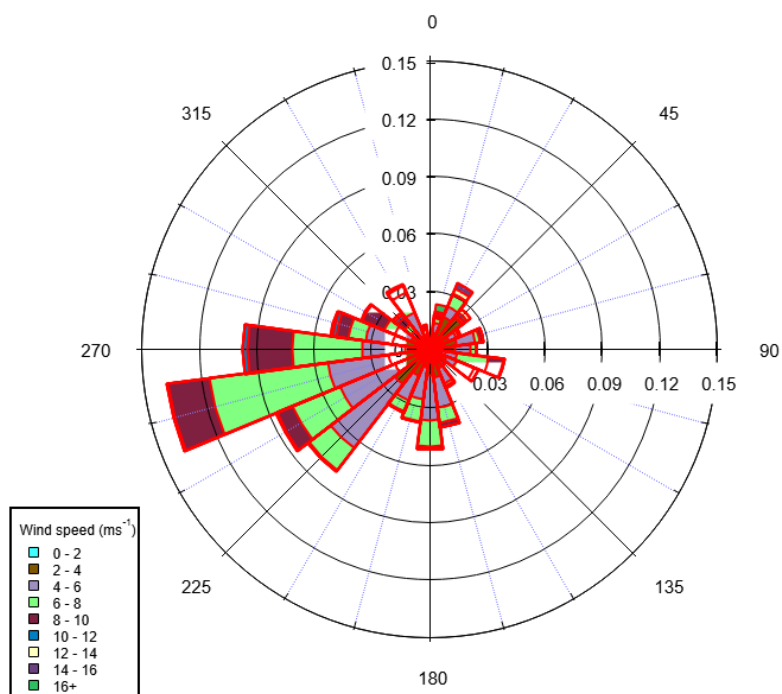
Figure 3. Wind rose plot for the entire campaign. Air originated from the SW sector (180°–270°) for approximately 50% of the time.
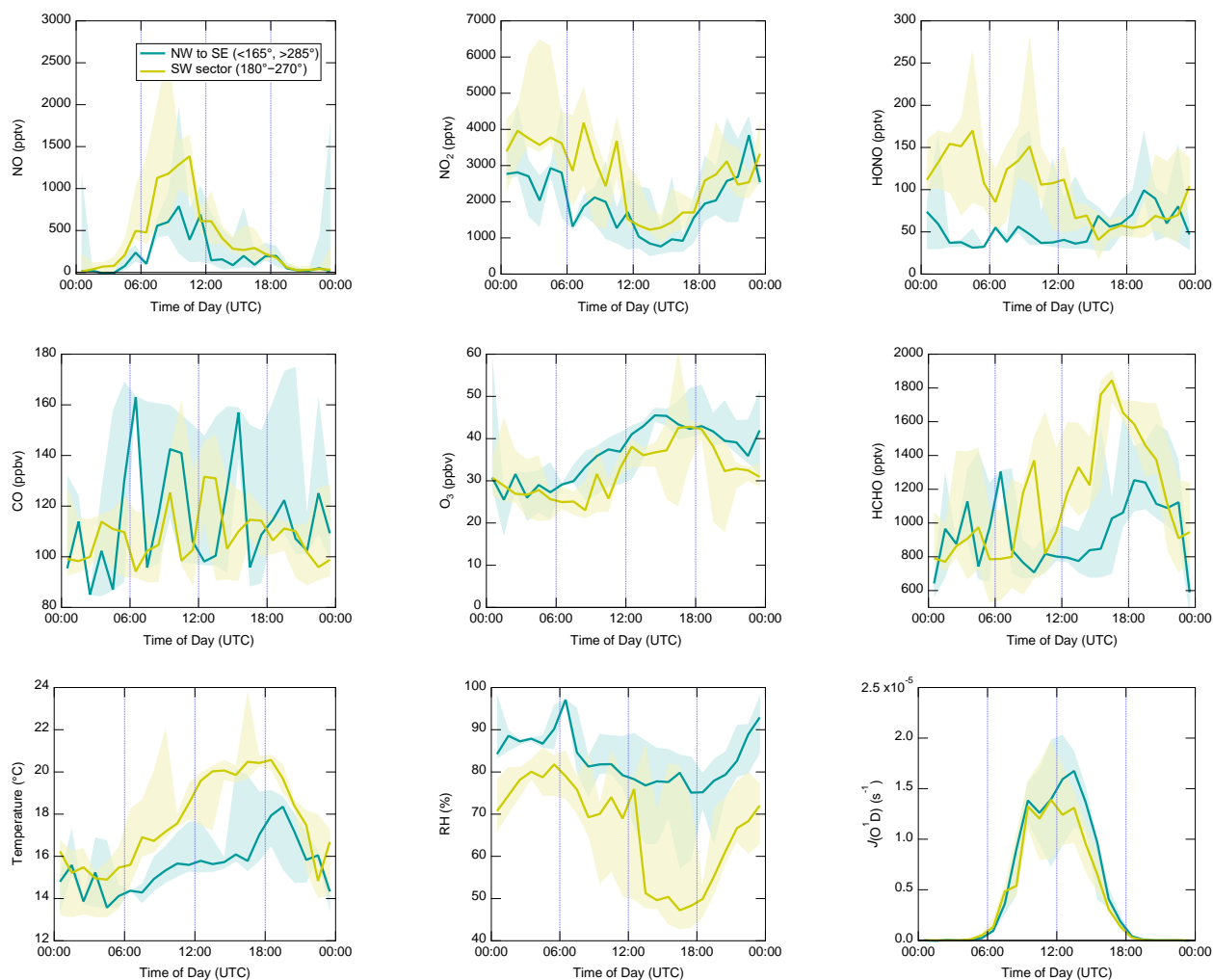
Figure 4. Diel profiles of trace gases and meteorological parameters, split according to wind direction (NW–SE = <165° and >285°; SW = 180°–270°). Data were only included if radical measurements were also available. Shaded areas correspond to 25th and 75th percentiles of the data in each time bin.
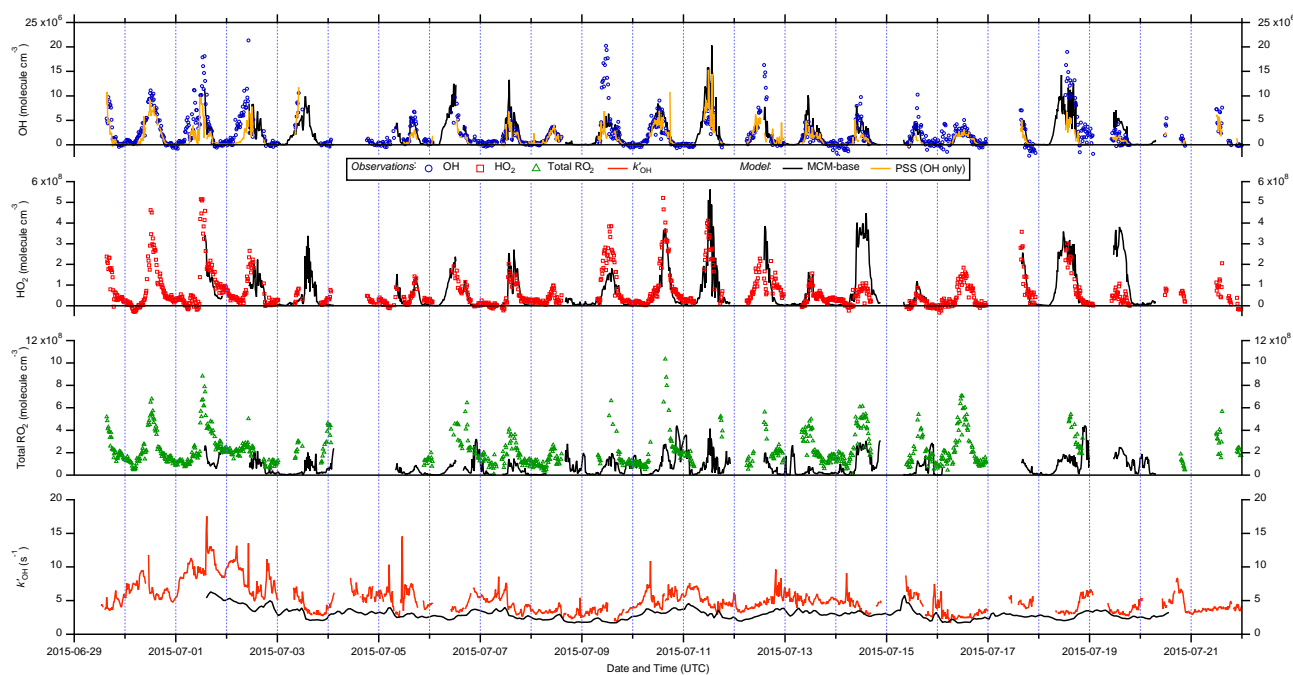
Figure 5. Time series of OH, HO$_2$, and total RO$_2$ measurements and comparison to MCM-base model and photostationary steady state (PSS) predictions. All data are at 15 min time resolution except for model OH reactivity (1 h). Error bars omitted for clarity.
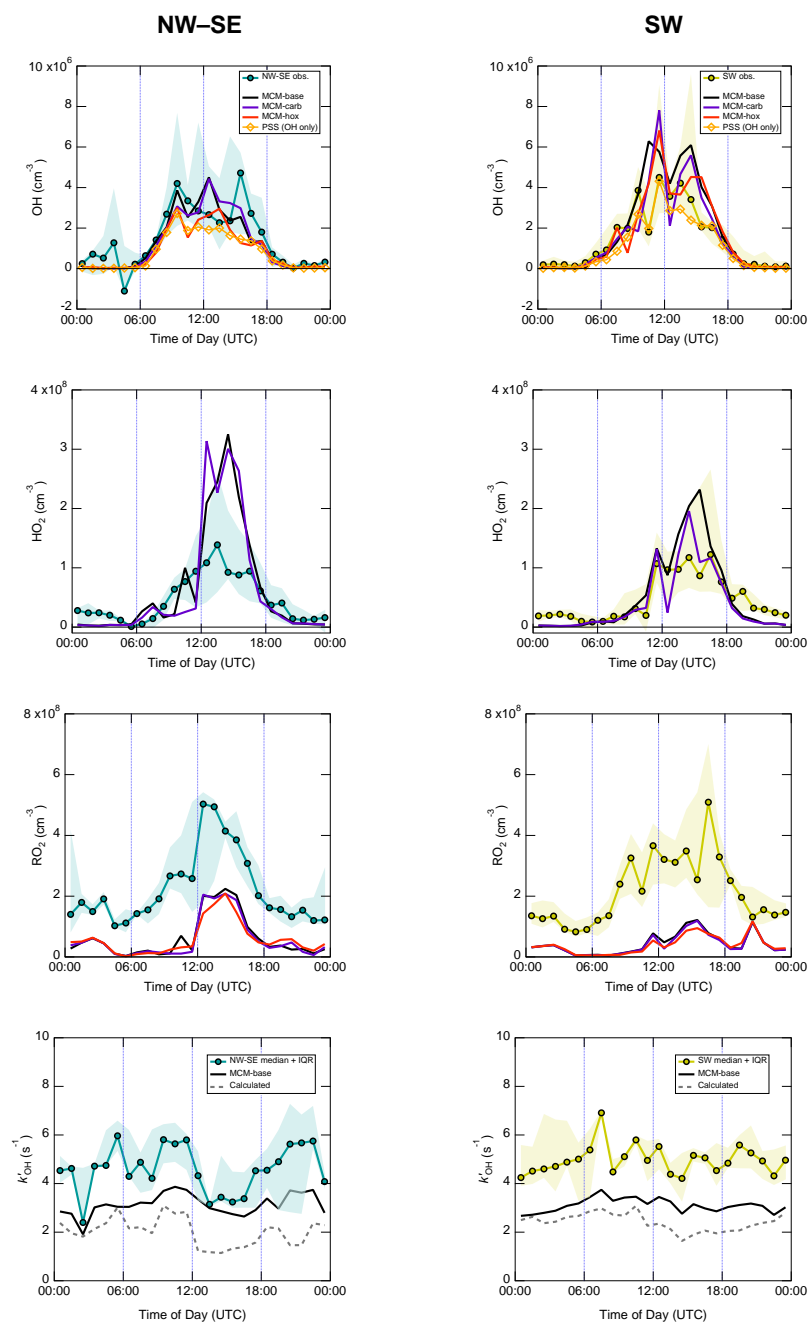
Figure 6. Hourly median diel profiles of OH, HO$_2$, total RO$_2$, and k'_{OH} and comparison to MCM-base and PSS model predictions, split according to wind direction (left NW–SE, right SW). Shaded areas correspond to 25th and 75th percentiles of the data in each time bin.
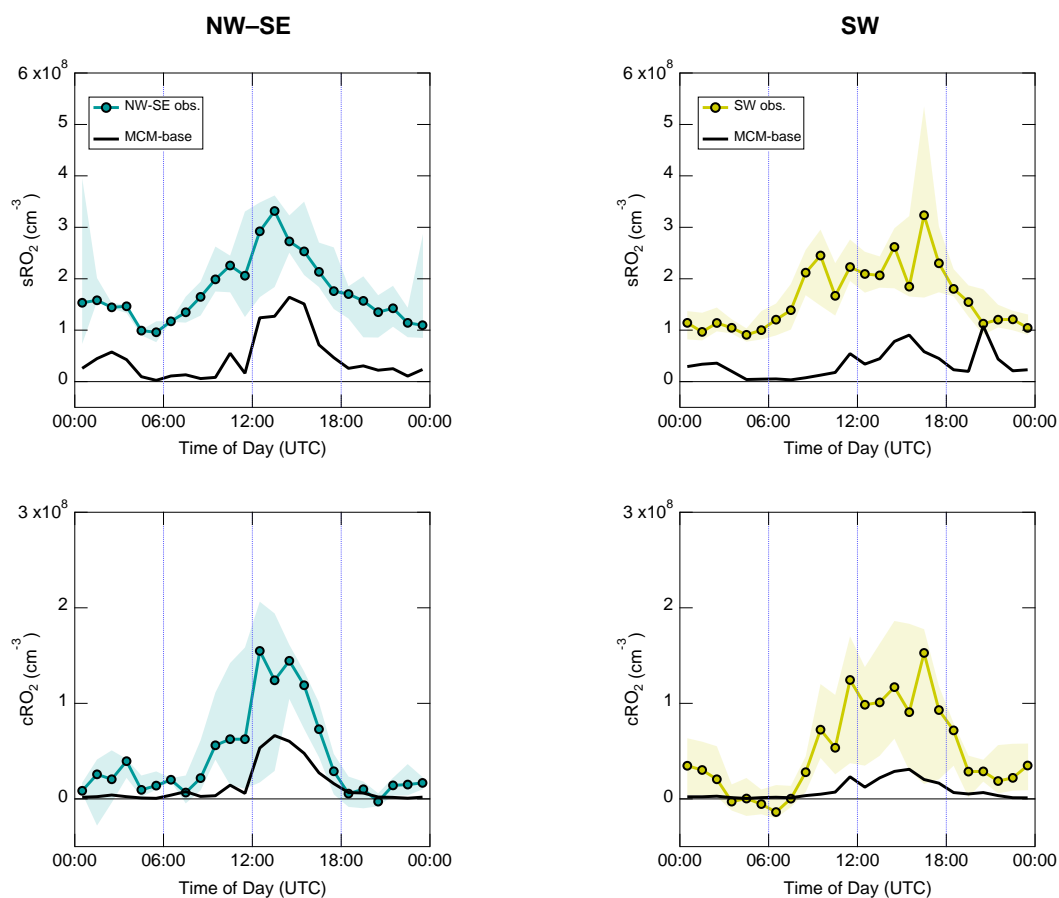
Figure 7. Hourly median diel profiles of "simple" (sRO$_2$) and "complex" RO$_2$ (cRO$_2$), defined in text, and comparison to MCM-base model predictions, split according to wind direction (left NW–SE, right SW).
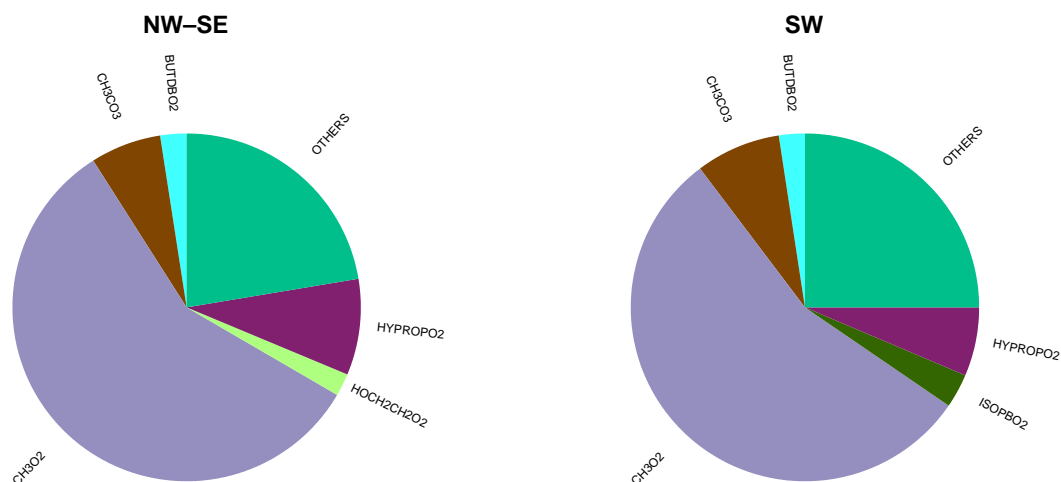
Figure 8. Daytime median RO_2 contributions predicted by the MCM-base model, split according to wind direction (left: NW–SE, right: SW). For clarity, only the top five RO_2 species are shown, otherwise the RO_2's are lumped together as "others". MCM nomenclature used, see text for definitions (Section 3.2).

5
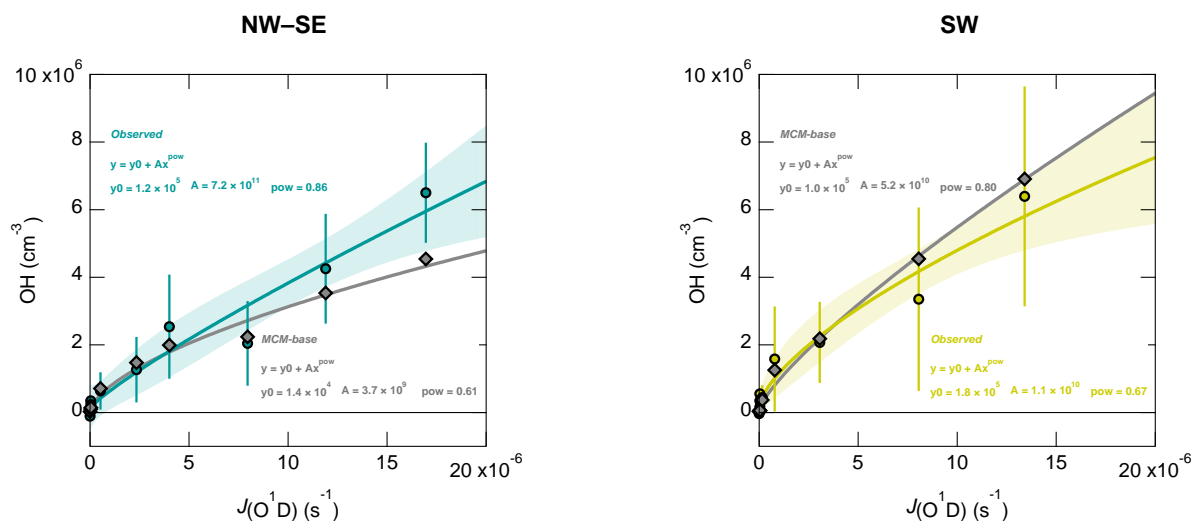
Figure 9. Observed and modelled OH binned against $J(O^1D)$ using 12 bins with approximately the same number of points, split according to wind direction (left NW–SE, right SW). Data are shown as means, where error bars on measurement points correspond to one standard deviation (SD, not shown for model data for clarity). Solid lines are power law fits to OH vs $J(O^1D)$, and shaded areas give 95% confidence intervals of the fits to observed data (not shown for model data for clarity).

10

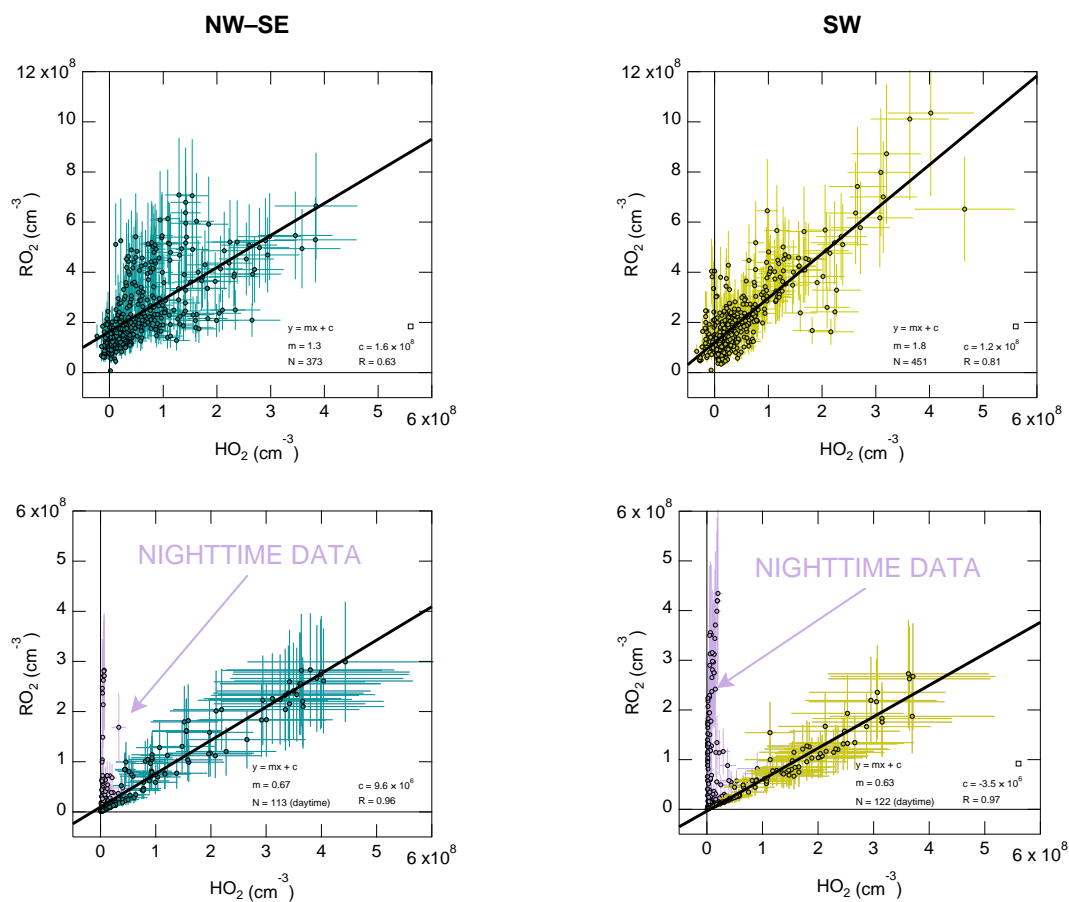**Figure 10.** Observed total RO_2 vs observed HO_2 (top) and modelled total RO_2 vs modelled HO_2 (bottom), split according to wind direction (left NW–SE, right SW). Solid black lines correspond to linear least squares fits. For the model results, nighttime data exhibit a different RO_2 vs HO_2 slope, highlighted in purple; these data were not included in fits.
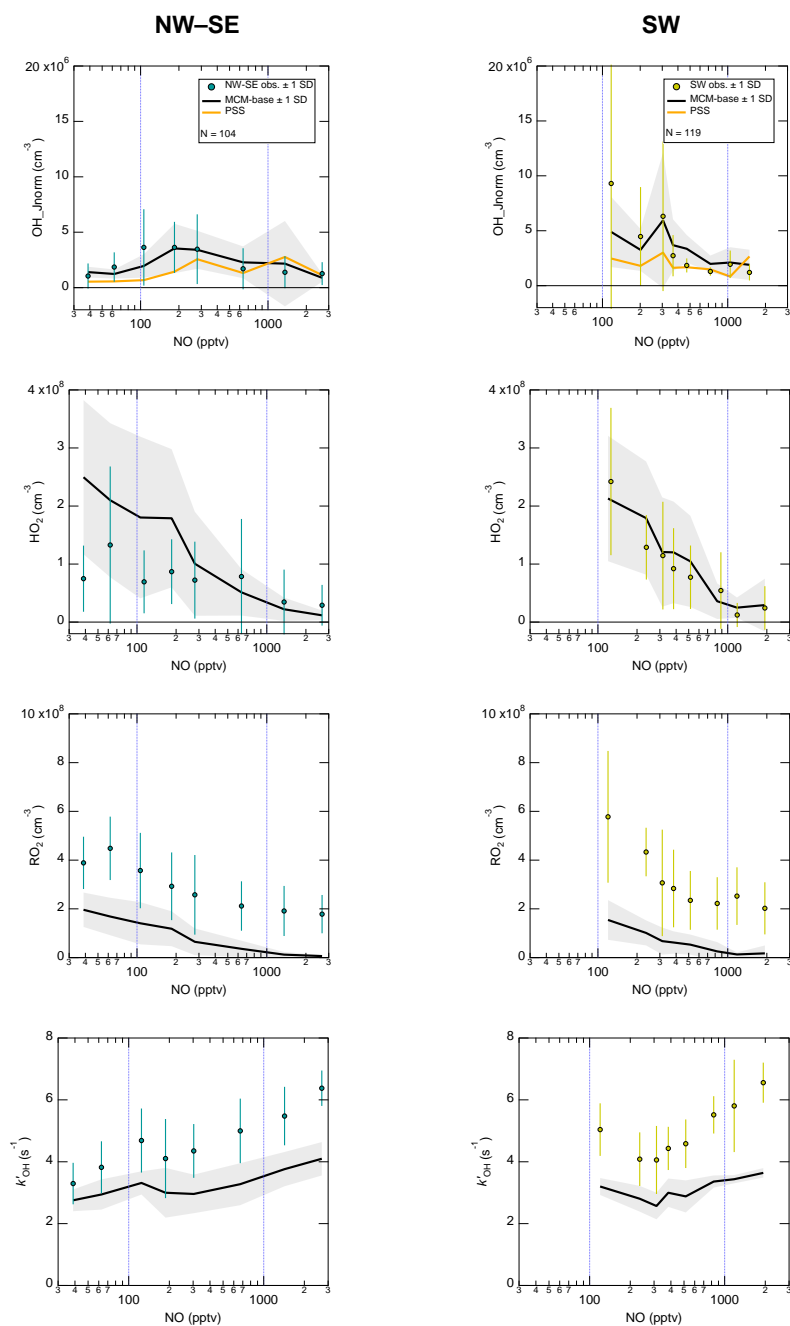
5

10

Figure 11. Dependence of observed and modelled OH (normalised to average $J(O^1D)$), HO_2, total RO_2, and OH reactivity on NO mixing ratios. Only daytime data were included, using the filter $J(O^1D) > 5 \times 10^{-7}$ s^{-1}. Data are shown as means $\pm$ 1 SD, and split according to wind direction (left NW–SE, right SW). Data were separated into 8 NO bins with approximately the same number of points.
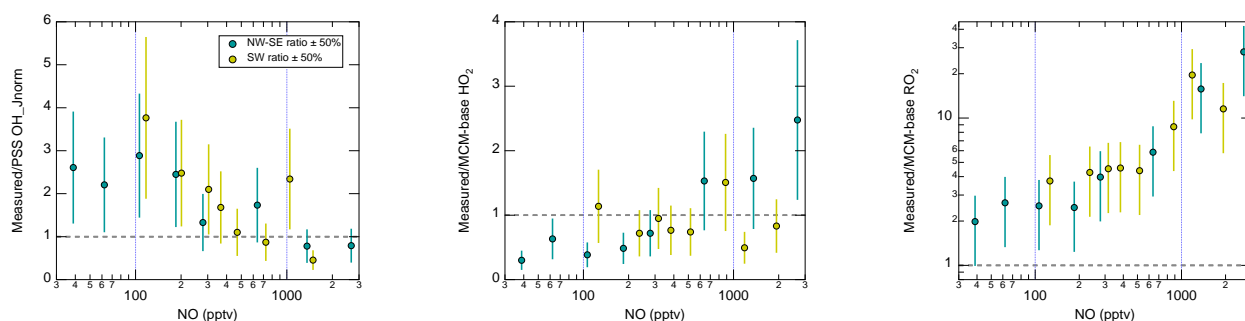
5

Figure 12. NO-dependence of the measurement-model ratios for radical species from Figure 11. Error bars correspond to an estimated combined measurement-model error of 50%. For OH, the reference model is the PSS calculation, and for HO_2 and RO_2 this is MCM-base. Note the *y*-log scale for RO_2.
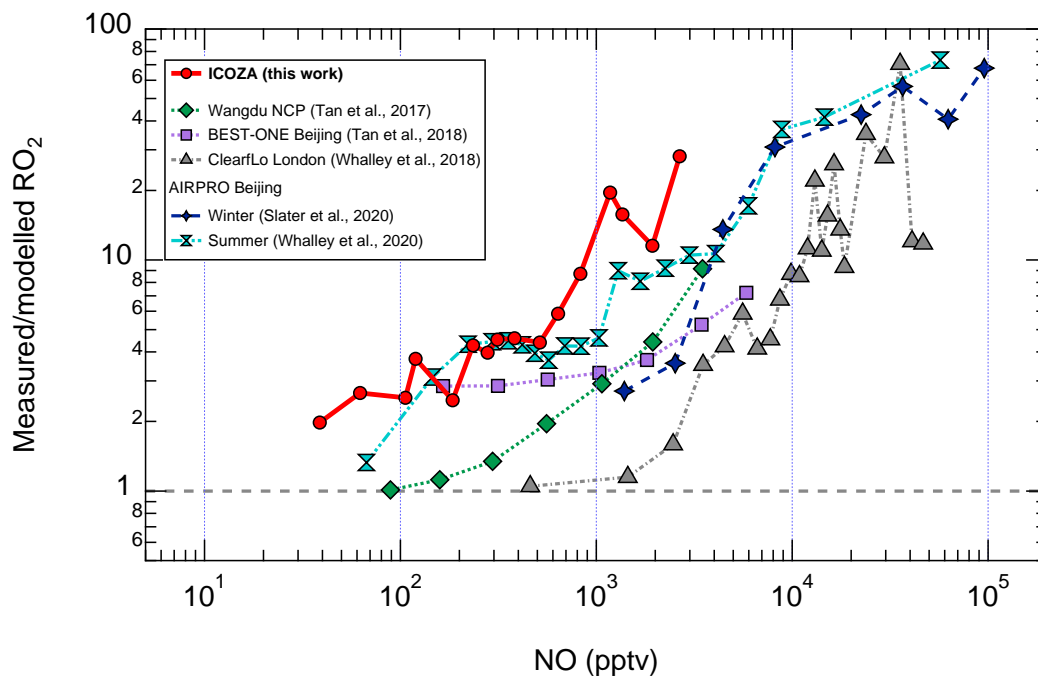

Figure 13. Comparison of RO_xLIF-measured RO_2 measurement-model ratios as a function of NO.
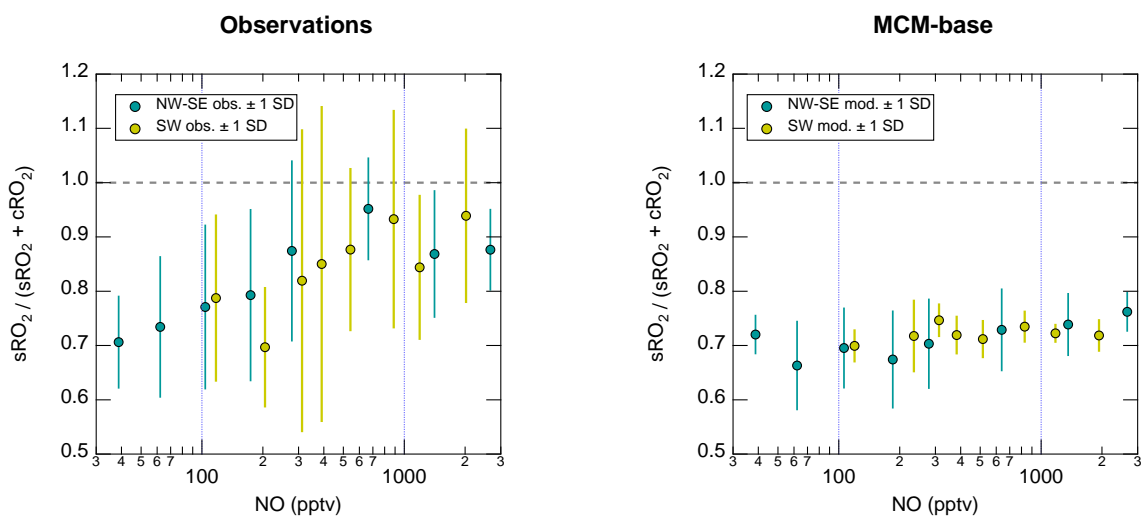
Atmospheric
Chemistry
and Physics
Discussions

Figure 14. Contribution of sRO_2 to total RO_2 (= sRO_2 + cRO_2) as a function of NO (measurements left, model results right). Data are shown as means ± 1 SD. Data were separated into 8 NO bins with approximately the same number of points.
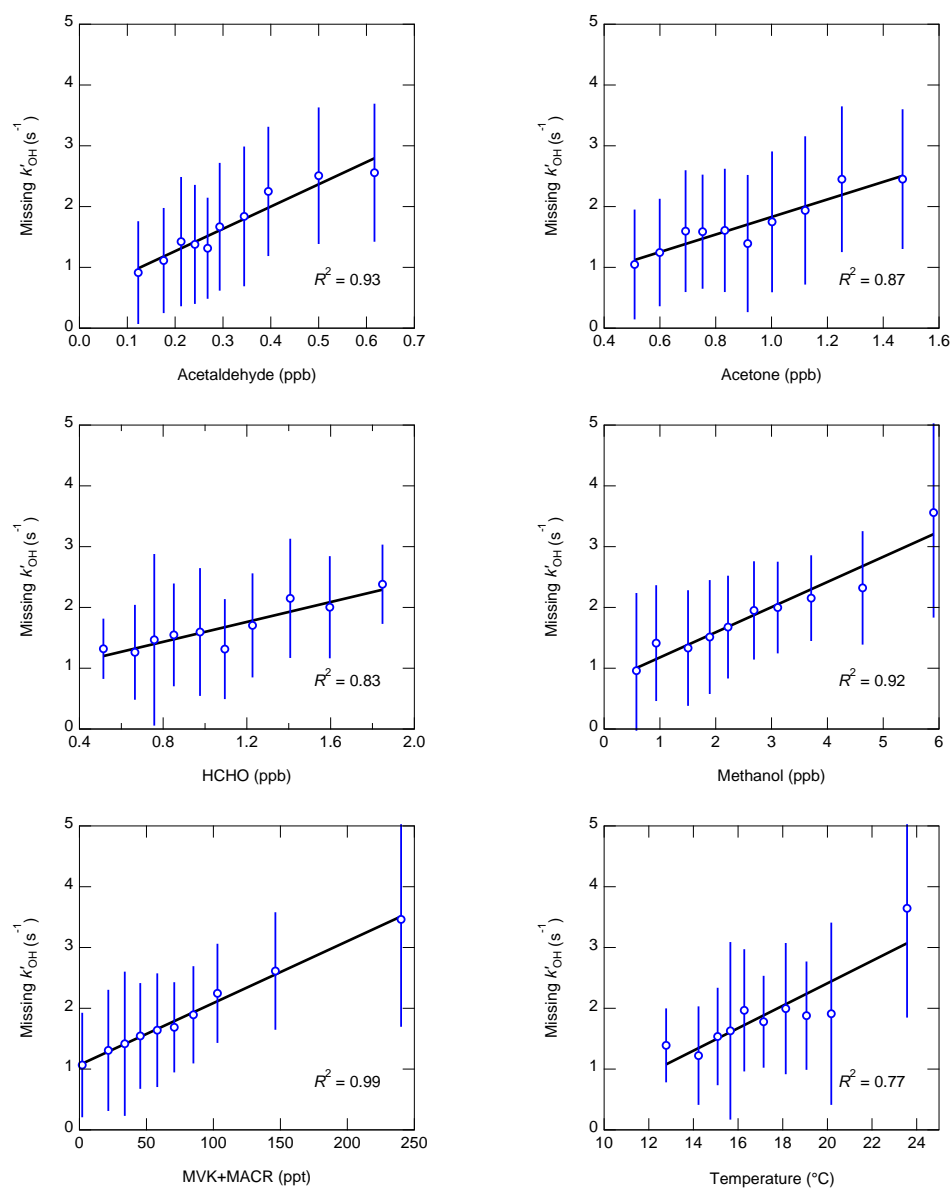
Atmospheric
Chemistry
and Physics
Discussions

Open Access

EGU

Figure 15. Dependence of missing OH reactivity on acetaldehyde, acetone, HCHO, methanol, MVK+MACR, and temperature. Data are shown as means ± 1 SD. In each plot, data were separated into 10 x-bins with approximately the same number of points.